Annu. Rev. Phys. Chem. 2002. 53:67–99
DOI: 10.1146/annurev.physchem.53.091001.094554

SCATTERING RESONANCES IN THE SIMPLEST CHEMICAL REACTION

Félix Fernández-Alonso[1] and Richard N. Zare[2]
[1]*Istituto di Struttura della Materia—Consiglio Nazionale delle Ricerche, Area della Ricerca di Roma—Tor Vergata, 00133 Rome, Italy; e-mail: felix@ism.rm.cnr.it; and*
[2]*Department of Chemistry, Stanford University, Stanford, California 94305-5080; e-mail: zare@stanford.edu*

Key Words transition state, quasibound states, scattering resonance, $H + H_2$ reaction family, reactive scattering, reaction dynamics

■ **Abstract** Recent studies of state-resolved angular distributions show the participation of reactive scattering resonances in the simplest chemical reaction. This review is intended for those who wish to learn about the state-of-the-art in the study of the $H + H_2$ reaction family that has made this breakthrough possible. This review is also intended for those who wish to gain insight into the nature of reactive scattering resonances. Following a tour across several fields of physics and chemistry where the concept of resonance has been crucial for the understanding of new phenomena, we offer an operational definition and taxonomy of reactive scattering resonances. We introduce simple intuitive models to illustrate each resonance type. We focus next on the last decade of $H + H_2$ reaction dynamics. Emphasis is placed on the various experimental approaches that have been applied to the search for resonance behavior in the $H + H_2$ reaction family. We conclude by sketching the road ahead in the study of $H + H_2$ reactive scattering resonances.

1. INTRODUCTION: FROM NUCLEAR PHYSICS TO CHEMICAL REACTIONS

Resonance behavior is ubiquitous in a wide range of physical phenomena. One of the most familiar examples comes from spectroscopy, where the energy of a photon $\hbar\omega$ is tuned to match the energy difference ΔE_{12} between two levels of an atom or molecule. The resulting energy spectrum is characterized by the appearance of sharp peaks (resonances) that obey the Bohr energy condition $\Delta E_{12} = \hbar\omega$. Likewise, the energy widths of these resonances may be associated with the lifetime of the excited state. These two quantities, line position and line shape, represent the most fundamental observables in atomic (1) and molecular (2) spectroscopy.

The behavior described above is not restricted to the use of photons as projectiles. In the 1930s, Fermi and collaborators noticed that slow neutron scattering had anomalously high cross sections at certain energies (3–6). These large capture

cross sections were interpreted by Bethe (7) and Bohr (8) in terms of the existence of quasistable states of the compound neutron-nucleus system at the resonance energies with lifetimes τ directly related to the peak energy widths Γ, i.e., $\tau = \hbar/\Gamma$. The energy dependence of the cross section in the neighborhood of an isolated narrow resonance followed the Breit-Wigner (9) formula

$$\sigma(E) \propto |A_{nr} + A_r|^2 = \left| A_{nr} + \frac{\Gamma}{(E - E_o) + i\frac{\Gamma}{2}} \right|^2 . \qquad 1.$$

Here E_o and Γ are the energy position and width of the resonance, and A_{nr} and A_r represent the nonresonant (direct) and resonant (indirect) contributions to the cross section. If direct scattering is negligible, the cross section has a Lorentzian energy profile with a width that is directly related to the lifetime of the compound state. This behavior, however, is not general, and the actual profile may show a variety of shapes, so-called Fano line shapes (10), depending on the destructive or constructive interference between the direct and indirect terms in Equation 1.

In the years following these initial findings, elementary particle resonances have been crucial for the understanding of the fundamental forces of nature. For example, pion-nucleon elastic scattering at low energies ~100–300 MeV is dominated by the so-called P_{33} resonance, a touchstone for the understanding of the strong nuclear force. This resonance has been entirely attributed to the formation of an excited nucleon state (11–13).

Some years had to pass between the firm establishment of resonance behavior in nuclear reactions and the experimental and theoretical verification of similar phenomena in atomic and molecular physics. In electron-atom/molecule scattering, resonances were discovered almost simultaneously by experiment and theory at the end of the 1950s, even though older measurements had already given some evidence of unexpected structure in scattering cross sections. In this sense, some authors (14, 15) consider the discovery of the Auger effect (16) as the first observation of a resonance in electron/heavy-particle scattering. Haas (17) and Schulz (18) measured significant structure in $e^- - N_2$ collision cross sections associated with vibrational excitation of the molecular target. These results were in good agreement with the theoretical expectations of Herzenberg & Mandl (19) using resonance theories. Similarly, experiments of Schulz & Fox (20) on $e^- - He$ collisions were successfully explained using a one-level Breit-Wigner formula by Baranger & Gerjuoy (21). Following these findings, a multitude of atoms and small molecules were investigated yielding numerous examples of the interaction of an incident electron with the target, resulting in temporary capture and subsequent decay (14, 15, 22–27).

It is worth emphasizing that such resonances are not simply of academic interest alone. The powerful infrared carbon dioxide laser, for example, is powered by efficient vibrational energy transfer from resonantly excited $N_2(v = 1)$ to CO_2 (28, 29). Recently, experimental evidence has been presented that double-strand breaks in DNA, caused by ionizing radiation incident on cells, arises from transient

molecular resonances induced by the secondary electrons at energies lower than the ionization potential (30). Thus, resonant scattering processes not only affect how some stars twinkle, but they also affect life processes.

In the late 1960s, several groups began the study of the role of scattering resonances and quasibound states in elastic and inelastic heavy-particle collisions using realistic models and specific molecular systems amenable to experimental investigation (30a–k). Using a statistical model for molecular collisions, Miller (30l) estimated the direct and resonant contributions to the cross section for the Cs + RbCl reaction. This chemical reaction was known to proceed via a long-lived intermediate from the scattering experiments of Herschbach and coworkers (30m). A more clear indication that scattering resonances would be important in chemical reactions came in the early 1970s when Truhlar & Kuppermann (31, 32) performed the first exact quantum-mechanical $H + H_2$ collinear computations. They observed that the total reactive and nonreactive cross sections displayed pronounced oscillations as a function of collision energy. The authors ascribed these features to the effect of interfering amplitudes for different semiclassical paths between reagents and products (32). Based on the results of close-coupling collinear calculations for the same reaction system, Levine & Wu (33) explicitly demonstrated the presence of resonances in reactive collisions. The surprising feature was the absence of a local minimum in the $H + H_2$ potential energy surface (PES) that could readily explain trapping during the course of reaction. The early $H + H_2$ classical trajectory studies of Hirshfelder, Eyring, & Topley (34) using the crude London-Eyring-Polanyi (35, 36) H_3 potential energy surface (PES) had noted the existence of long-lived trajectories owing to temporary trapping in a local minimum at the saddle point region (which has been called "Lake Eyring"). Such a minimum was later shown to be an artifact in the earlier $H + H_2$ PES arising from a sign error (37–39). It was not present in the one used for these calculations. Levine & Wu (33) explained these resonances in terms of the strong coupling between the relative motion along the reaction coordinate and the internal degrees of freedom of the compound triatomic molecule. Owing to such couplings, the structure in the reaction cross section could be accounted for in terms of quasibound states that arise from internal excitation with lifetimes on the order of 30 fs. Subsequent work by Wu et al. (40–42) on collinear $H + H_2$ and model A + BC reactions provided strong evidence for the existence of the dynamical Lake Eyring under a wide range of circumstances. In addition, resonances were clearly observed whenever the effect of changing the vibrational frequency along the reaction coordinate gave rise to adiabatic potential wells. This oversimplified picture of reactive resonances has been extremely useful in further investigations and has served as a basis for many approximate treatments that followed. Concurrent with these efforts, Schatz & Kuppermann (43) analyzed in detail the oscillations in their calculated reactive cross sections for collinear $H + H_2$ at total energies of 0.90 eV and 1.276 eV. A calculation of scattering phase shifts, delay times, and Argand diagrams (a plot of the imaginary and real parts of the reactive amplitudes as a function of collision energy) enabled an interpretation of these features in terms of compound-state

(Feshbach) resonances. This work appears to be the first time that the term Feshbach resonance, originally coined for nuclear processes (44, 45, 45a), was utilized in the context of chemical reactions to denote quasibound states associated with a PES that possesses no local minima and thus is not capable of supporting bound states.

The world of collinear collisions of course does not describe accurately the real world. Would resonance scattering behavior still be prominent for three-dimensional scattering? Schatz & Kuppermann (46) answered this question in the affirmative. They showed that resonance peaks were reduced in magnitude but persisted in two- and three-dimensional (total angular momentum $J = 0, 1$) calculations. The energy shifts observed in going from lower to higher dimensionality were consistent with the addition of the zero-point-energies of the bending degrees of freedom of the H_3 complex. Further details of the developments on the dynamics for the $H + H_2$ reaction in this early period may be found in the review by Truhlar & Wyatt (47). These early studies showed that scattering resonances were not as uncommon in chemical reactions as initially thought, even in the three-dimensional world. Unfortunately, carrying out fully converged, three-dimensional calculations in a reliable manner had to wait more than a decade owing to the need to develop efficient algorithms for their calculation and the need for more powerful computers. The early work had established, however, that a study of the resonance spectrum of a chemical reaction could provide a means of investigating the structure of the transition state region of elementary chemical reactions [see the review by Kuppermann (48)].

During this initial period, a number of approximate methods for describing reactive resonance scattering were developed and tested on the two benchmark reactions, $H + H_2$ and $F + H_2$. The goal of this work was to develop simplified yet realistic models that allowed for the solution of a lower-dimensionality problem via quantal and semiclassical adiabatic treatments in natural (49, 50), hyperspherical (51–53), and Jacobi collision coordinates (54–56) [see also the reviews by Bowman (57, 58)]. By adiabatic we mean that the motions of the slow modes are frozen, and the resulting equations of motion solved with this constraint. This work met with some success. It was able to reproduce and provide a physical explanation for previous (and often obscure) computational results. The classical approach to reaction dynamics of Child & Pollak (59–63) stimulated the study of the correspondence between quantum mechanical resonances and classical mechanics in terms of resonant periodic orbits (RPOs). An RPO corresponds to an unstable periodic path along the PES. Trajectories starting close to an RPO have a tendency to be guided along it, thereby causing temporary trapping of the system and enhanced energy transfer between the reactant and product valleys. The location of these RPOs for collinear $H + H_2$ collisions matched with quantitative accuracy the quantal resonance energies (50, 64). Pollak and coworkers (53, 55, 65) tested the approach further for isotopic variants of the same reaction and showed the reliability of the method for the prediction of resonance energies. Resonances appeared near the energetic thresholds of new vibrational channels. The RPO

approach was successfully extended to three-dimensional calculations (66, 67). The method, however, has been the subject of some criticism; see, for example, Hipes & Kuppermann (68) as well as Pollak (67).

A new impetus for theoretical calculations arose at the end of the 1980s with the experimental report by Valentini and coworkers of Feshbach resonances in the state-resolved integral cross sections (ICS) for the $H + H_2$ (69, 70) and $D + H_2$ (71) reactions. These experiments produced fast H or D atoms by photolysis and detected the resulting molecular reaction product by coherent anti-Stokes Raman scattering (CARS). [See also Reference (72) for a review of $H + H_2$ experiments carried out prior to the 1990s]. The resonances reported in these experiments appeared to be in agreement with previous quantum mechanical calculations for low values of the total angular momentum J (46, 56, 68, 73–75). The first fully converged (J up to 31) three-dimensional calculations on the $H + H_2$ reaction by Zhang & Miller (76, 77) showed, however, a dramatic blurring of the resonance peaks once all partial waves were computed. The same effect was observed for the isotopic variant of this reaction $D + H_2$ (78). Calculations by a number of other groups (79, 80) corroborated the theoretical results of Zhang & Miller. Moreover, photoinitated experiments using resonance enhanced multiphoton ionization (REMPI) for molecular product detection by Zare and coworkers (81), showed no structure in the state-resolved integral cross sections. Miller (82) has presented an excellent review of this brief yet intense period in $H + H_2$ reaction dynamics. In subsequent work, Miller & Zhang (83) made detailed calculations of state-resolved integral and differential cross sections (DCS) for the $H + H_2$ and $D + H_2$ reactions for total energies up to 1.4 eV. Although resonances were not discernable in the integral cross sections, they distinctly appeared in the energy dependence of state-resolved differential cross sections in the form of a ridge in the energy-angle (E–θ) plane. Such a ridge was related to the dependence on J of the resonance energy and was used to provide the rotational constants and lifetimes of the compound triatomic complex. The resonances seen in these calculations were broad in energy, thereby providing an explanation for their absence in state-resolved integral cross sections. It is interesting to note that quasiclassical trajectory (QCT) calculations for the $D + H_2$ reaction by Aoiz and coworkers (84–86) also showed resonance ridges similar to the ones previously ascribed to a purely quantum mechanical effect. These findings suggest that these features may have an important semiclassical interpretation, one that needs further explication.

By the early 1990s, two important conclusions were reached for further studies on the $H + H_2$ reaction: (*a*) It is not advisable to draw strong conclusions from a comparison between scattering experiments and the results of partial calculations, that is, the need exists to perform an extensive database of fully converged quantum mechanical calculations on this reaction system. (*b*) The signatures of scattering resonances are likely to be most easily found in experiments that measure the energy dependence of fully state-resolved differential cross sections.

The $H + H_2$ reaction family invites detailed study because it is for this reaction system that the PES can be most accurately calculated. Beginning in the 1960s

with the appearance of the Porter-Karplus PES (37), outstanding progress has been made. To date, a number of accurate PESs have appeared: the Liu-Siegbahn-Truhlar-Horowitz PES (LSTH) (87–89), the double-many-body-expansion PES (DMBE) of Varandas and coworkers (90), and more recently the Boothroyd-Keogh-Martin-Peterson PESs (BKMP and BKMP2) (91, 92) as well the Exact-Quantum-Monte-Carlo PES (EQMC) of Wu et al. (93), of which the latter is estimated to have an accuracy of better than 4 cm^{-1}. At the same time, time-dependent and time-independent scattering calculations have advanced where it is possible to obtain all scattering attributes in the context of motion on a single potential energy surface.

It is important to stress that from an experimental point of view the operational definition of a resonance is a scattering feature that changes sharply as a function of the total energy of the reaction system and which may be associated with metastability of the compound system. This is the sense in which experimentalists search for resonances, as has been seen in past work on nuclear and electron scattering. On the other hand, theoretical calculations are needed to understand what causes the resonance in the scattering process. In this sense, theory and experiment are complementary. To illustrate this definition we refer to the recent crossed-beam experiments and QM calculations of Liu and coworkers on the $F + HD \rightarrow HF + D$ reaction (94–97) that have firmly established the existence of resonance features in the ICS of a chemical reaction. $F + HD$ ICSs have also been complemented with energy- and angle-resolved measurements (95) that display sharp backward-forward variations with collision energy. In addition, similar studies by Dong et al. (98), Chao & Skodje (99), and Sokolovski & Castillo (100) have once more revived the long-standing issue regarding resonance signatures in the angular distributions of the $F + H_2$ reaction (101), whose origin goes back to the ground-breaking experiments of Lee and coworkers in the mid-1980s (102, 103). At present, the $F + H_2$ reaction is far less well understood than the $H + H_2$ reaction and a fully quantitative comparison between experiment and theory has been hampered by deficiencies in our present knowledge of the underlying PES. The resonances reported by Liu and coworkers provide a benchmark measurement to tune the electronic structure calculations for the FH_2 reaction system. For a review, see Liu (97).

This realization of how to search for resonances has inspired three independent efforts in the $H + H_2$ reaction family in the past decade:

1. Wrede & Schnieder (104) used photoinitiated crossed-beam techniques to search for predicted resonance structure over a narrow energy range. They were able to obtain state-resolved integral and differential cross sections for the $H + D_2(v = 0, j = 0) \rightarrow HD(v' = 0, 1; j') + D$ between 1.27 eV and 1.30 eV. They achieved outstanding resolution but they found no resonances.
2. Kendrick et al. (105, 106) also examined the $H + D_2$ reaction in which $HD(v' = 0, j' = 7)$ was detected in a velocity-sensitive manner, from which the integral cross section was estimated between a collision energy of 0.73 eV

and 1.02 eV. They observed a bump (~50% variation) in the integral cross section that agreed well with their calculations (partial waves up to J = 6). Subsequently, the calculations have been extended to higher partial waves, and the resonance feature is no longer present (107–109).

3. Zare and coworkers (110, 111; B. D. Bean, F. Fernández-Alonso, J. D. Ayers, A. E. Pomerantz, R. N. Zare, unpublished results) have measured state-resolved differential cross sections for the reaction of $H + D_2 \rightarrow HD(v' = 3, j') + D$ between 1.39 eV and 1.85 eV using photoinitiation in which the angular distribution is derived from the law of cosines (113, 114). They observed strong forward scattering for the $HD(v' = 3, j' = 0)$ product but not for $HD(v' = 3, j' > 2)$. Moreover, the amount of forward scattering varied sharply with collision energy.

Following a discussion of the nature of reactive scattering resonances, we shall return to possible interpretations of these experiments.

2. CLASSIFICATION OF REACTIVE SCATTERING RESONANCES

This section provides a taxonomy of reactive resonances. We make a special effort to connect formal definitions of scattering resonances with approximate treatments of reactive scattering.

2.1. Shape Resonances

Our starting point for a discussion of reactive resonances is the reaction coordinate *s*, by which we mean the motion along the minimum energy path (MEP) in a given PES. Motion along a direction ρ transverse to *s* can be assigned to the internal coordinate of our reactive system. These concepts can be put on a firmer basis for a collinear collision between three atoms using natural collision coordinates as first introduced by Marcus (115, 116) and extensively discussed in References (117–120). In natural collision coordinates, *s* asymptotically approaches the asymmetric stretch motion of the three-atom complex. It ultimately leads to the breakage of chemical bonds. Similarly, motion along ρ corresponds to the symmetric-stretch mode. We assume that reactions can be thought to proceed primarily along the MEP.

Let us forget momentarily about the existence of ρ motion and concentrate on the one-dimensional MEP potential energy profile. Such a profile may look like what is shown in Figure 1*a* with a well around $s = 0$ indicating the existence of a quasibound state at a particular energy below the barrier top. The situation depicted in Figure 1*a* is similar to what the first PESs predicted for the $H + H_2$ reaction (Lake Eyring). It is known to be present in other reactive systems as, for example, the ion-molecule reaction $He + H_2^+$, isoelectronic with $H + H_2$ (121–123). The one-dimensional Schrödinger equation describing the

motion along the energy profile V_{MEP} (s) in Figure 1*a* is given by

$$\frac{\partial^2\psi}{\partial s^2} + \frac{2\mu}{\hbar^2}[E - V_{MEP}(s)]\psi = 0, \qquad 2.$$

where is μ the reduced mass and E the total energy of the system. A plane wave with positive energy incident from the left gives rise to a reflected wave (back to reagents) and a transmitted wave (forward to reaction products). The corresponding boundary conditions for the solution of Equation 2 may then be written as

$$\psi(s = -\infty) = e^{iks} + S_R e^{-iks} \qquad 3a.$$

and

$$\psi(s = \infty) = S_T e^{iks}, \qquad 3b.$$

where $k = \sqrt{2\mu E/\hbar}$ is the wavevector, and S_R and S_T are the (complex) energy-dependent reflection and transmission amplitudes. The transmission coefficients (reaction probabilities) are obtained by computing $|S_T|^2$. Figure 1*b* shows the resulting transmission coefficient as a function of incident energy. Owing to the presence of the well, we observe a sharp peak below the maximum of the potential caused by a close match in energy between the incident energy and a quasibound (quantized) level. In the context of reactive scattering we attribute this peak to what is called a shape resonance, i.e., the shape of the interaction potential is responsible for the presence of structure in the reaction cross section. In formal scattering theory, S_R and S_T are elements of the scattering S matrix. All observables related to the scattering process may be computed from knowledge of this quantity (124). In particular, resonances are associated with poles in the S matrix in the fourth quadrant of the complex energy plane. Referring back to Equation 1, we can associate a pole in such an expression with the complex energy $E = E_0 - i\frac{\Gamma}{2}$ that causes the denominator of the resonant contribution to the cross section to vanish. This feature is perhaps the most discriminating definition of a scattering resonance. From a theoretical viewpoint, a study of resonance scattering reduces to the search for such poles in the complex plane. In the language of complex analysis, the S matrix is an analytical function. Consequently, knowledge of the location of the poles of the S matrix completely defines the S matrix and hence, completely characterizes the scattering process (124, 125). In this light, all scattering may be regarded as arising from scattering resonances. But this way of regarding the scattering process may not be useful or insightful if the resonance widths overlap appreciably.

Other ways exist for ascertaining the resonance character of the sharp peak shown in Figure 1*a*. In Figure 1*b* we also show the time delay associated with the passage along the MEP. The desired time delay may be obtained from the S matrix by use of the expression (126)

$$\tau = \mathrm{Im}\left(\hbar\frac{1}{S_T}\frac{dS_T}{dE}\right), \qquad 4.$$

where Im denotes the imaginary part. The time delay τ as a function of energy shows a pronounced delay at the resonance energy indicative of a long residence time inside the potential well. Depending on the depth and width of the well shown in Figure 1*a*, the reaction cross section may show a number of peaks, indicative of the presence of several quasibound (quantized) levels. The depth of the well could also be below the asymptotic energy of products and reagents, indicative of the existence of a stable molecule (bound states). Such is the case of the $O + H_2$ reaction that has the water molecule as its intermediate (stable) state (127). It is known through unimolecular decomposition experiments that in this case structure persists even above the well, at energies associated with virtual levels of the intermediate (128, 129).

2.2. Barrier Resonances

In a recent study, Friedman & Truhlar (130) have posed a very intriguing question: Are chemical reaction barriers resonances? Using a methodology very similar to the one we have used for our description of shape resonances, they were able to show that symmetric energy barriers are also associated with poles in the S matrix. To illustrate this fact, they demonstrated the possibility of effecting a continuous change from a barrier resonance to a shape resonance (see Figures 1*a* and 1*b*). A hint for this behavior can already be observed in Figure 1*b*. It shows a small bump in the time delay near the top of the barrier but smaller and broader than the one we ascribed to a shape resonance. In Figures 1*c* and 1*d* we show the solution to the one-channel scattering problem for an Eckart barrier (131) that closely resembles the $H + H_2$ MEP, as calculated by Friedman & Truhlar (130). The transmission probability rises smoothly, but we can also observe a broad peak in the time delay associated with energies close to the potential barrier. Classically, it corresponds to metastability associated with passage through a potential maximum, but more interestingly, it is associated quantum mechanically with an S-matrix pole far removed from the real energy axis. Such a pole possesses a large imaginary energy component, which implies that it corresponds to a short-lived metastable state. Subsequent work by Truhlar and coworkers (132) on asymmetric one-dimensional potentials corroborated the above conclusions for a number of asymmetric potential functions. A similar pole structure of the S matrix for parabolic and Eckart potential barriers has also been discussed by Seideman & Miller (133), and Ryabov & Moiseyev (134) in the context of transition state theory and the calculation of reaction probabilities. In their approach, reaction rate expressions are given in terms of Siegert eigenvalues, that is, the complex eigenvalues of the Schrödinger equation with outgoing boundary conditions at energies where the poles occur (135). These Siegert eigenstates have been traditionally associated with scattering resonances (15, 136, 137). Seideman & Miller (133) have contended, however, that the progressions of poles associated with barriers do not bear a direct relationship with conventional (isolated) scattering resonances as they are used to describe direct dynamics. We note, however, that a distinction between isolated and overlapped resonances is not a sharp one,

and as will be further explained below, barrier resonances do enjoy many of the characteristics of conventional resonances.

Let us consider the properties of a harmonic barrier (a completely soluble problem by analytical methods) (133, 134, 138). Similar conclusions apply to other analytically solvable problems such as Eckart barriers (133, 134, 139). The poles associated with the barrier are infinite in number and accumulate at the energy of the barrier top. Their precise values are given by

$$E_r = E_o - i\hbar\omega(2n+1), \quad n = 0, 1, 2\ldots, \qquad 5.$$

where E_o is the position of the barrier and ω its frequency. As shown by Equation 5, the leading pole occurs at $n = 0$, and it is the longest-lived (smallest imaginary part). Atabek et al. (138) have shown that these simple harmonic barriers can lead to localization effects similar to those found in the usual resonance phenomenon.

Skodje and coworkers (140–144) have presented extensive evidence for the existence of such barrier resonances in collinear and three-dimensional calculations for the $H + H_2$ reaction family. In their computational method, a wave packet is launched in the transition state region. The Fourier transform of the wave packet temporal decay shows structure directly attributable to the participation of metastable states. Collinear studies on $D + H_2$ displayed a complicated resonance spectrum (143). Three different types of peaks were found and identified according to the following categories: conventional reactive resonances, barrier resonances, and threshold anomalies (Wigner cusps). The last of these were easily identified in their method because they became arbitrarily small as the resolution of the calculation was increased. The other two cases, however, corresponded to the formation of true metastable states. A total of ten barrier states dominated the lower energy part of the spectrum, between 0.525 eV and 2.268 eV, and formed two progressions along the reactant and product channels. Similar to conventional resonances in this reaction system (Feschbach resonances; see Section 2.3), their stability also increased with energy. Semiclassically, they were associated with maxima in the vibrationally adiabatic potential curves, that is, repulsive periodic orbit dividing surfaces (PODS), in contrast with the RPOs related to conventional resonances.

Motivated by the need to interpret these barrier resonances, Sadeghi & Skodje (143, 144) have derived an analytic expression for parabolic barrier resonances using a time-dependent formalism. For the lowest even wavepacket, it takes the form

$$S(\Omega) \propto \prod_{k=0}^{\infty} \left(\frac{\left(\frac{1}{2} + 2k\right)\omega}{\Omega + i\left(\frac{1}{2} + 2k\right)\omega} \right), \qquad 6.$$

where $\Omega = E/\hbar$, and ω is the barrier frequency. The denominator of this expression is reminiscent of the pole positions for the harmonic barrier shown in Equation 5: There is a contribution of an infinite number of poles located at $\Omega = -i(\frac{1}{2} + 2k)\omega$. These line shapes have been successfully applied to the barrier resonances appearing in the collinear $D + H_2$ reaction (143, 144). Varandas & Yu have also

observed these barrier resonances in time-dependent wavepacket calculations for the H + H_2 (145), Mu + H_2/D_2 (146, 147), and H + DH/D + HD (148) reactions.

2.3. Feshbach Resonances

Our previous discussion on shape and barrier resonances was strictly one-dimensional in nature, although even the simplest atom-diatom reaction involves more than one degree of freedom. It is precisely the energy exchange between various collective modes of the compound molecule that are responsible for what is commonly called Feshbach resonances. We have already mentioned their importance in chemical reactions and, in particular, for the explanation of resonances in the H + H_2 reaction. In this section, we provide a simple model that serves as an illustration of the origin of this effect.

Let us consider a one-dimensional potential like the one used in our discussion of shape resonances (Section 2.1). In the present example, this interaction potential still represents the passage between reagents and products, e.g., the minimum energy path with a potential energy profile $V_{MEP}(s)$. If we add a second degree of freedom ρ perpendicular to the reaction path whose interaction potential depends parametrically on the position along s, the Hamiltonian becomes

$$H = -\frac{\hbar^2}{2\mu_s,}\left(\frac{\partial^2}{\partial s^2}\right) - \frac{\hbar^2}{2\mu_\rho}\left(\frac{\partial^2}{\partial \rho^2}\right) + V_{MEP}(s) + V(\rho; s), \qquad 7.$$

where the μ_s and μ_ρ represent the reduced masses for s and ρ motions, respectively. For simplicity, we assume a harmonic potential $V(\rho; s) = \frac{1}{2}\mu_\rho\omega(s)\rho^2$. The harmonic frequency $\omega(s)$ is taken to be smallest at $s = 0$ as an indication of bond weakening at the point of switching between reagents ($s < 0$) and products ($s > 0$). We proceed to solve this very crude model for a chemical reaction taking the motion along s to be slow compared to the one along ρ (in the spirit of the Born-Oppenheimer separation of electronic and nuclear motions). Such an approximation amounts to neglecting the first kinetic energy term in Equation 7. The resulting Schrödinger equation is

$$\left(-\frac{\hbar^2}{2\mu_\rho}\left(\frac{\partial^2}{\partial \rho^2}\right) + V(\rho; s)\right)\varphi(\rho, s) = (\varepsilon_n(s) - V_{MEP}(s))\varphi(\rho, s), \qquad 8.$$

where $\varepsilon_n(s) = \hbar\omega(s)(n + \frac{1}{2}) + V_{MEP}(s)$ are the eigenenergies associated with the harmonic motion perpendicular to the reaction path. The total wave function can be calculated from a series expansion in terms of the solutions of Equation 8,

$$\Psi(\rho, s) = \sum_m \Phi_m(s)\varphi_m(\rho, s). \qquad 9.$$

We seek to solve the Schrödinger equation

$$\left(-\frac{\hbar^2}{2\mu_s}\left(\frac{\partial^2}{\partial s^2}\right) - \frac{\hbar^2}{2\mu_\rho}\left(\frac{\partial^2}{\partial \rho^2}\right) + V_{MEP}(s) + V(\rho; s)\right)\Psi(\rho, s) = E\Psi(\rho, s). \qquad 10.$$

After substitution of Equations 8 and 9 into 10, we find

$$\left(-\frac{\hbar^2}{2\mu_s}\left(\frac{\partial^2}{\partial s^2}\right)+\varepsilon_n(s)+\sum_m A_{nm}\right)\Phi_n(s)=E\,\Phi_n(s), \qquad 11.$$

where the matrix elements of A_{nm} are given by

$$A_{nm}=-\frac{\hbar^2}{2\mu_\rho}\left(2\left\langle\varphi_n\left|\frac{\partial}{\partial s}\right|\varphi_m\right\rangle\frac{\partial}{\partial s}+\left\langle\varphi_n\left|\frac{\partial^2}{\partial s^2}\right|\varphi_m\right\rangle\right). \qquad 12.$$

For a harmonic potential describing motion transverse to the reaction coordinate, the matrix elements in Equation 12 are given by (40)

$$\left\langle\varphi_n\left|\frac{\partial}{\partial s}\right|\varphi_m\right\rangle=\left(\frac{1}{2}\frac{d\ln\omega(s)}{ds}\right)\cdot\left\{\left[\frac{m(m-1)}{4}\right]^{1/2}\delta_{nm-2}-\left[\frac{(m+1)(m+2)}{4}\right]^{1/2}\delta_{nm+2}\right\}, \qquad 13.$$

and

$$\left\langle\varphi_n\left|\frac{\partial^2}{\partial s^2}\right|\varphi_m\right\rangle=\left(\frac{1}{2}\frac{d\ln\omega(s)}{ds}\right)^2\cdot\left\{\left[\frac{m(m-1)(m-2)(m-3)}{16}\right]^{1/2}\delta_{nm-4}-\frac{(m^2+m+1)}{2}\delta_{nm}+\left[\frac{(m+1)(m+2)(m+3)(m+4)}{16}\right]^{1/2}\delta_{nm+4}\right\}$$
$$+\left(\frac{1}{2}\frac{d^2\ln\omega(s)}{ds^2}\right)\cdot\left\{\left[\frac{m(m-1)}{4}\right]^{1/2}\delta_{nm-2}-\left[\frac{(m+1)(m+2)}{4}\right]^{1/2}\delta_{nm+2}\right\}, \qquad 14.$$

Equations 13 and 14 show that, in the spirit of this simple model, the A_{nm} matrix can effect transitions between vibrational adiabatic states differing by two and four quanta.

By considering only the diagonal elements of the A_{nm} matrix, we arrive at the following first-order approximation

$$\left(-\frac{\hbar^2}{2\mu_s}\frac{\partial^2}{\partial s^2}+\varepsilon_n(s)+\frac{\hbar^2}{16\mu_\rho}(n^2+n+1)\left(\frac{d\ln\omega(s)}{ds}\right)^2\right)\Phi_n(s)=E\,\Phi_n(s). \qquad 15.$$

Equation 15 has a very simple interpretation: motion along s takes place with an effective potential

$$V_{eff}(s) = V_{MEP}(s) + \hbar\omega(s)\left(n + \frac{1}{2}\right) + \frac{\hbar^2}{16\mu_\rho}(n^2 + n + 1)\left(\frac{d\ln\omega(s)}{ds}\right)^2. \quad 16.$$

The first term in Equation 16 is the original MEP along the reaction coordinate. The presence of a second (coupled) degree of freedom has the effect of adding a vibrational energy (vibrationally adiabatic correction) plus a diagonal correction to the energy. The interplay between these two terms can be strong enough to modify greatly the shape of the potential. Also, the energy corrections to the original MEP increase with vibrational quantum number. In this manner, new Lake Eyrings may appear once the interaction of the various degrees of freedom of the system are taken into account. Such is the case of the H + H_2 reaction. We note that the interaction between internal degrees of freedom can be sufficiently large to yield deep wells lying below the ground state adiabatic potential curve (that is, they are true bound states of the system). In this situation we speak of vibrational bonding. This issue has been extensively discussed in the literature in the context of heavy-light-heavy triatomics where the rapid motion of the light atom acts as the binding force (149–156).

At this point, we can begin to use the concepts discussed in the context of shape and barrier resonances. Feshbach resonances associated with adiabatic potentials may have shape and/or barrier character. This behavior depends on which features of the effective interaction potential are responsible for the temporary trapping of the system. As an example of a realistic situation, we show in Figure 2 the first three vibrationally adiabatic potentials for the H + H_2, D + H_2, and H + D_2 reactions using the computer program of Truhlar and coworkers, ABCRATE (157) on the DMBE PES (90). These curves represent the J = 0 adiabatic potential curves, taking into account the energies of all the internal modes of the triatomic species in three dimensions (one symmetric stretch v_{str} and two degenerate bends v_{bend}). In all three cases, we can clearly discern the appearance of potential wells in the vibrationally adiabatic potentials near the transition state region ($s = 0$). Also, the potentials for the isotopic variants D + H_2 and H + D_2 are not symmetric owing to the different reagent and product mass combinations. This asymmetry will likely manifest itself as a preference for metastable states to be localized in the reagent or product side, depending on the nature of the resonance. The H + D_2 reaction does not show potential wells up through $v_{str} = 2$, which suggests that the observation of metastable states will occur at higher collision energies. Indeed, Garrett et al. (50) have predicted the absence of low-energy reactive resonances for this system owing to the lack of resonance energy levels for $v_{str} = 0, 1, 2$. The adiabatic potential curves shown in Figure 2 correspond to J = 0. It is possible to compute similar adiabatic potential curves for an arbitrary total angular momentum J by addition of the rotational energy of

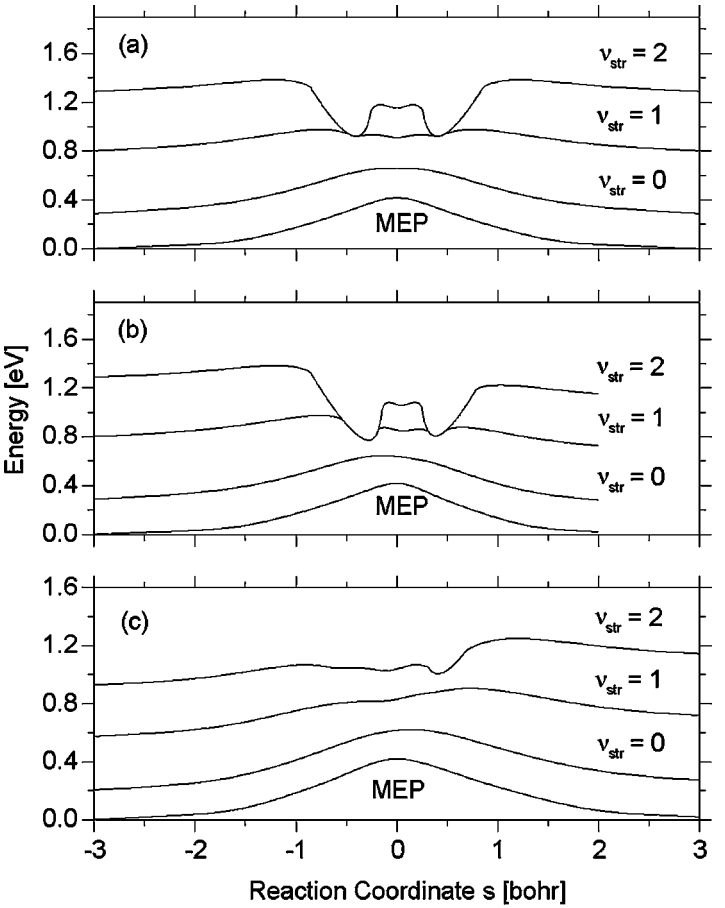

Figure 2 Three-dimensional (J = 0) vibrationally adiabatic potentials for (*a*) H + H_2; (*b*) D + H_2; and (*c*) H + D_2.

the triatomic complex. Under the rigid rotor approximation it takes the form

$$E_{rot} = B_{rot}(s)J(J+1) = \frac{\hbar^2}{2I(s)}J(J+1), \qquad 17.$$

where I(s) is the moment of inertia of the triatomic complex.

We show in Figure 3 the effect of adding the energy given by Equation 17 to the $v_{str} = 3$ adiabatic potential for the H + D_2 reaction for values of the total angular momentum that are known to participate in reactive scattering below 2.0 eV (J < 35). Aside from the more pronounced appearance of metastable potential wells, we observe the presence of potential barriers both on the reagent and product sides of the reaction. Both features may be responsible for the presence of Feshbach resonances associated with adiabatic wells and barriers at energies

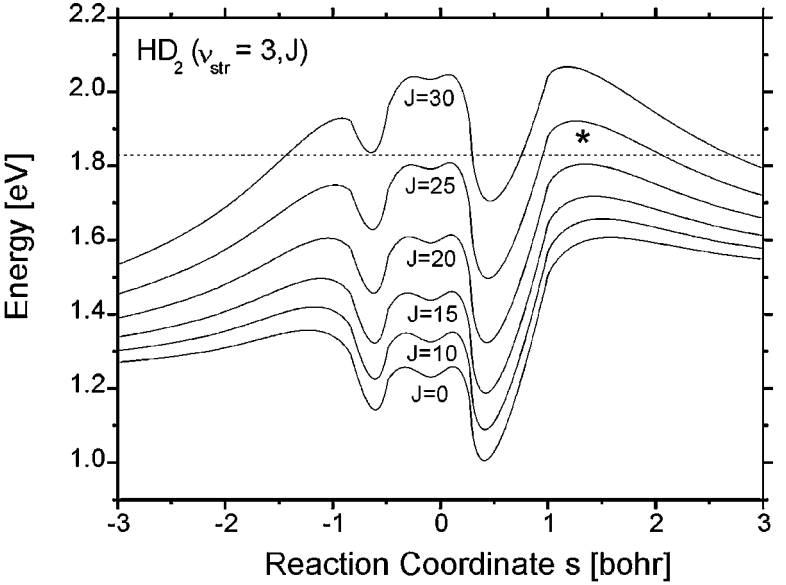

Figure 3 Adiabatic potential for $H + D_2$ ($v_{str} = 3$) as a function of the total angular momentum J = 0, 10, 15, 20, 25, and 30 using Equation 17. The horizontal dashed line marks the total energy of the experiments $E_{tot} = 1.83$ eV, and the asterisk the location of the energy barrier thought to be responsible for trapping (see Section 3.3).

between ~1.4 eV and ~2.0 eV. This example is particularly relevant to developing a simple picture for resonances in the $H + D_2 \rightarrow HD(v' = 3, j') + D$ reaction (see next section).

To illustrate the importance of Feshbach resonances associated with barriers, we comment on their relation to new formulations of transition state theory. Recent theoretical work strongly suggests that the overall reactivity of a chemical reaction (the reaction rate) is directly related to the presence of quantized bottlenecks that control the passage of reactive flux to products (158–160). This approach to rate theories has been successfully tested using accurate three-dimensional quantal calculations for an extensive number of atom-diatom systems including $H + H_2$ (161–165), $D + H_2$ (166), $F + H_2$ (167, 168), $O + H_2$ (164, 165, 169–171), $H + O_2$ (172–174), Cl + HCl, I + HI, I + DI (175), $Cl + H_2$ (176), $He + H_2^+$ (177, 178), and $Ne + H_2^+$ (179, 180). In this context, reaction thresholds associated with maxima of vibrationally adiabatic curves have been related to barrier resonances. Although isolated narrow resonances arising from conventional trapped states (wells) are assigned using a full set of triatomic quantum numbers (v_1, v_2^K, v_3) corresponding to the symmetric v_1, bend v_2, vibrational angular momentum K, and asymmetric stretch motion v_3 (56, 68, 73, 181, 182), threshold or barrier transition states have been consistently labeled by (v_1, v_2^k), that is, they are missing the asymmetric stretch

quantum number v_3 associated with the reaction coordinate. Truhlar and coworkers (159) have suggested that such a missing degree of freedom may be recovered if it is identified with the dominant barrier pole as, for example, by setting $n = 0$ in Equation 5. More rigorously, Zhao & Rice (183) have identified transition states with scattering resonances using complex scaling techniques.

3. RESONANCES IN THE H + D_2 REACTION: RECENT PROGRESS, CURRENT STATUS, AND FUTURE PROSPECTS

Only in the last decade have experiments been capable of measuring state-resolved differential cross sections as a function of collision energy. This task has been made possible by the use of lasers. H or D atoms are generated by laser photolysis of suitably chosen precursors. The reaction products are detected again with lasers, using either atomic (184) or molecular (185) Rydberg-tagging or, alternatively, by REMPI of the HD product (186–188).

For the H + H_2 family, special attention has been given to the H + D_2 reaction. Theoretical efforts to carry out extensive and accurate calculations on this particular reaction system have been more or less synchronous with experiment. Prior to the experiments to be described in this section, quantal calculations for the H + D_2 reaction were scarce. D'Mello et al. (189) were the first to calculate well-converged integral cross sections at collision energies of 0.55 and 1.3 eV. Their results compared favorably with the photoinitiated and state-resolved experiments of Zare and coworkers (190). Prior to this work, calculations for the H + D_2 system had been restricted to low values of the total angular momentum (75, 191, 192).

Moreover, theoretical calculations had neglected the incorporation of geometric phase (GP) effects [for a review of GP effects in molecular systems, see Yarkony (193) and Mead (194)]. In the H + H_2 reaction system, GP effects arise from the existence of a conical intersection between its two lowest adiabatic PESs (195–200). As the nuclei perform a closed loop around this intersection, the electronic wave function is forced to change sign if it is to remain real-valued. Such a purely quantum mechanical effect, which may be called a dynamical Jahn-Teller effect, is expected to influence the reaction dynamics in a fundamental way even at energies that are well below the energy at which the two PESs intersect ($\sim$2.7 eV). Whenever reaction products can be scattered into the same solid angle element by direct scattering and by a scattering mechanism that involves a pseudorotation about the conical intersection, it is necessary to sum the two scattering amplitudes and square them to obtain the reaction probability. In such circumstances, constructive and destructive interference occurs in the DCS. Moreover, such GP effects can persist in the integral cross section even after a partial-wave summation. Calculations by Kuppermann and coworkers showed this behavior to hold for the H + H_2 (195–197), D + H_2 (197, 198), and H + D_2 (199, 200) reactions. As Baer (201) and others have stressed, GP effects are part of the nature of the scattering process. Their inclusion is not a matter of choice. GP effects are expected to play an important

role in the dynamics of many bimolecular reactions as well as unimolecular decompositions (202–206).

3.1. Crossed-Beam Experiments in Search of Resonances; The Role of Geometric Phase

In the past few years, Schnieder and collaborators have carried out a series of very elegant high-resolution crossed-beam experiments for the $H + D_2$ reaction. Their experimental setup consists of two parallel, spatially separated molecular beams. One beam contains HI as the photolytic precursor for fast H atoms. The other beam contains the diatomic reagent D_2. Laser photolysis of HI generates H atoms with a well-defined laboratory spatial distribution. The laser polarization is chosen so as to direct this H-atom beam toward the D_2 beam. D-product detection is achieved with meV resolution by use of Rydberg atom tagging (184). An analysis of the kinetic energy spectrum of the D product as a function of scattering angle provides the desired HD(v′, j′) product state resolution. This experimental arrangement trades off signal production for energy resolution. More details about the experimental technique can be found in recent reviews by Liu (97) and Casavecchia and coworkers (207, 208).

Kuppermann & Wu (199) predicted for the LSTH PES a pronounced reactive scattering resonance at a total energy of 1.481 eV (1.29 eV collision energy) for the state-specific exchange $H + D_2(v = 0, j = 0) \rightarrow HD(v' = 0, j' = 4, 5) + D$ only if GP was included in the calculation. Guided by these predictions, Wrede & Schnieder (104) measured D-atom angular distributions between 1.27 and 1.30 eV, but they found no evidence for the predicted resonance structure. Instead, their experimental results were in good agreement with QM calculations on the LSTH PES at 1.30 eV by D'Mello et al. (189) that did not include GP effects. It was argued (104) that such a lack of agreement could be caused by inaccuracies of the LSTH PES used in the calculations of Wu & Kuppermann, which could shift the resonance energy by as much as 13 meV, that is, outside of the collision energy range investigated in the experiments.

Based on the results of the experiments of Wrede & Schnieder (104) and the calculations of Kuppermann (199), it appears that the influence of geometric phase on $H + H_2$ scattering dynamics is a very sensitive function of collision energy as well as the form of the PES. It seems true, however, that at some collision energies GP effects essentially make no contribution to the scattering dynamics. This absence of GP effects might result from the lack of collision trajectories that make a closed loop around the conical intersection. At present, the experiments of Schnieder and coworkers for the $H + D_2$ reaction have been compared with converged NGP (NGP = not including GP effects) QM calculations on the LSTH and on the newer BKMP2 surfaces at collision energies of 0.5 eV (209, 210), 1.28 eV (209, 211), 2.2 eV (212, 213), and 2.67 eV (214). The agreement between the two is very good, including the last collision energy of 2.67 eV, which lies slightly above the conical intersection for the $H + H_2$ system.

Recent QM calculations by Kendrick (215, 216) have shown that for the H + D_2 reaction, GP effects beautifully cancel out for the first six partial waves and for total energies between 0.4 and 2.4 eV. These conclusions are valid for both the BKMP2 and LSTH PESs. It is unlikely that higher partial waves will behave in a different way, but to date no fully converged GP calculations have been completed. The cancellation of GP effects calculated by Kendrick is so astonishing that we wonder whether a simple explanation exists to account for it. To date, no answer to this important question has been put forward. Xu & Varandas (217) and Mahapatra et al. (218) reported a similar absence of GP effects in their calculations.

In addition, Kendrick's calculations showed broad transition-state resonances in the rotationally resolved integral and differential cross sections obtained from a consideration of these first few partial waves. It is still possible, but we believe not likely, that the true PES will show more pronounced GP effects. Wu et al. (93) have developed a new Exact Quantum Monte Carlo (EQMC) PES that the authors claim to be one order of magnitude more accurate than previous ones. A comparison of converged QM mechanical calculations on the EQMC PES with experiment has not yet been performed. It would be very desirable, however, to have a calculation of cross sections and resonance positions including GP effects on this new PES and to compare them with previous work. At this point, we conclude that no general consensus has been reached on the effects of GP and their impact on the reaction dynamics and resonance spectrum for this chemical reaction. It seems clear, however, that GP effects are minor for the H + D_2 reaction over the collision energies so far investigated.

We expect GP to be important under some reaction conditions, and past experiments on the integral cross section for D + $H_2(v' = 1, j' = 1)$ (219) suggest this may be the case (198), but more work, experimental and theoretical, is needed before this effect can be claimed to be quantitatively understood. We note that the computational effort required to incorporate GP effects in scattering calculations is considerable. This difficulty may be overcome once recent and efficient timedependent methods for the solution of the reactive scattering problem (220) are utilized.

3.2. An Old Problem Revisited: Does Resonance Structure in the Integral Cross Section Survive Partial-Wave Summation?

Recent photoinitiated experiments by Shafer-Ray and coworkers (105) have indicated the existence of resonance structure in the integral cross section for the state-specific reaction H + $D_2 \rightarrow$ HD($v' = 0, j' = 7$) + D at a collision energy of 0.94 eV. The GP QM calculations on which the comparison with theory had been made included only the first seven partial waves ($J < 7$). Conventional wisdom based on a large body of calculations for this reaction system, as well as other isotopic variants, has brought these results into question. It now seems clear that after summation of partial waves up to $J = 30$–35, no structure remains in the ICS energy dependence for the HD($v' = 0, j' = 7$) product state (106). This conclusion has been independently obtained from the NGP QM calculations of Chao et al. (107), Aoiz et al. (108), and Kendrick (109).

Kendrick (109) has analyzed in detail how partial wave summation affects state-resolved ICSs and DCSs for the $H + D_2$ reaction. Owing to its heavier mass, the $H + D_2$ reaction system is a more favorable case for the survival of resonance features in the ICS than its isotopic cousins $H + H_2$ and $D + H_2$, which Miller & Zhang (83) showed a decade ago to be devoid of them. The most distinct peaks in $H + D_2$ state-resolved ICSs occur for the vibrationless and rotationless product state. Oscillations in the ICS become very faint and difficult to detect experimentally for $v' > 1$ and/or $j' > 3$. Much more interesting are the ICSs for the vibrationally excited reaction $H + D_2(v = 1, j = 0) \rightarrow HD(v', j') + D$ that display very clear resonance bumps. Experimental work along these lines would be very timely in order to corroborate these predictions. Vibrationally excited D_2 may be obtained by stimulated-Raman-pumping (SRP) techniques (219, 221–226). Moreover, ICSs are far less difficult to measure than DCSs, and the wealth of information to gain from them appears to make efforts in this direction worthwhile.

It is tempting to offer some reassessment of the ICS measurements by Valentini and coworkers on $H + p\text{-}H_2$ (69, 70) and $D + H_2$ (71). Our confidence in fully converged theoretical calculations has advanced to the point that the features they observed cannot be attributed to structure in the ICS as a function of collision energy. We do know, however, that resonances occur for low partial waves in the energy range they investigated. Their observations might be explained as arising from a partial selection of scattering angles. It is very easy to imagine that the experiments discriminated in favor of slow-moving, backward-scattered molecular products. This discrimination could be caused by the time delay between photo-initiation and CARS detection as well as by the spatial overlap of photolysis and probe laser beams. Theory teaches us that these backward-scattered products correlate to a large extent with low-J partial waves (small impact parameters). Thus, the observation of such products defeats the blurring of resonance structure arising from partial-wave summation. Possibly, the first observations of scattering resonances were made by Valentini and coworkers, but unfortunately, it is not possible to quantify with ease what exactly was observed.

3.3. Forward Scattering in the $H + D_2 \rightarrow HD(v' = 3, j') + D$ Reaction

The photoloc approach, as recently developed by Zare and coworkers (113, 114, 227, 228), represents an alternative and promising approach to crossed-beam experiments for the measurement of state-resolved integral and differential cross sections for the hydrogen exchange reaction. Its name stems from the two major elements of the technique: first, laser photolysis initiates the chemical reaction in a free-jet expansion of a photolytic precursor (such as HBr or HI) and reagent (D_2); second, the law of cosines is used to relate the product laboratory velocity distribution to the center-of-mass differential cross section. Using REMPI detection of the $HD(v', j')$ product and the core-extraction technique (229), Fernández-Alonso et al. (228, 230, 231) have measured product-state-resolved DCSs for the $HD(v' = 1)$ and $HD(v' = 2)$ vibrational manifolds at collision energies of 1.70 eV and 1.55 eV,

respectively. Comparison with converged QM calculations on the BKMP2 PES shows good agreement with experiment (232). The shift from backward scattering toward sideways scattering observed with increasing product rotational angular momentum was interpreted as a tendency for the reagent orbital angular momentum to be channeled into product rotation. Such a trend is consistent with a direct reaction mechanism and is also very clear in the crossed-molecular-beam data of Schnieder and coworkers (104, 209–214).

Subsequent measurements of $H + D_2 \rightarrow HD(v' = 3, j') + D$ DCSs at a collision energy of 1.64 eV (110) have shown for the first time clear deviations from the direct behavior previously observed for other $HD(v', j')$ product states. A large forward-scattering peak was observed for low-j' product states as shown in Figure 4 . Quasiclassical trajectory (QCT) calculations at this collision energy (110) indicated some forward scattering but failed to reproduce its magnitude. An analysis of the classical trajectories associated with forward scattering features revealed a very different underlying reaction mechanism involving large values of the total angular momentum of approximately $J = 20$ (impact parameters of 0.70–0.80 Å) and time delays on the order of 26 fs (see Figure 5). These time delays are still well below the rotational period of the HD_2 complex, thereby explaining why the angular distribution lacks forward-backward symmetry. Analysis of single forward-scattered trajectories demonstrated a preference for an early elongation of the D_2 chemical bond causing the appearance of potential wells about the HDD collinear configuration that leads to temporary trapping of the complex. These observations were in agreement with a classical model for $H + H_2$ resonances previously proposed by Muga & Levine (233).

These experimental findings and first attempts to explain forward scattering in this reaction have stimulated further theoretical studies. Truhlar and coworkers (234) have used a simplified vibrationally adiabatic model in the same spirit as that discussed in Section 2.3, to provide a quantum mechanical interpretation of the resonance signatures found in the $HD(v' = 3, j' = 0)$ angular distributions. The resonance was associated with an $HD_2(v_1 = 3, v_2 = 0, J = 20)$ complex localized on a vibrationally adiabatic barrier on the product side (see Figure 3). The predictions of this reduced-dimensionality quantum mechanical study were in very good agreement with the previous conclusions reached from the analysis of quasiclassical trajectories (110). Based on previous theoretical predictions for the $H + H_2$ reaction (162, 165), the assignment $v_2 = 0$ was consistent with the observation of the largest amount of forward scattering for the rotationless state $HD(v' = 3, j' = 0)$.

As a continuation of this line of work, Zare and coworkers (111; B.D. Bean, F. Fernández-Alonso, J.D. Ayers, A.E. Pomerantz, R.N. Zare, unpublished results) have measured $HD(v' = 3, j')$ DCS's between 1.39 eV and 1.85 eV in order to characterize in more detail forward-scattering features. Figure 6 presents the observed $HD(v' = 3, j' = 0)$ time-of-flight profiles as a function of collision energy along with a comparison with NGP QM predictions (F.J. Aoiz, L. Bañares, J.F. Castillo, B.D. Bean, F. Fernández-Alonso, et al., unpublished results). The agreement between the two is very satisfactory. In particular, at $E_{col} =$

1.64 eV the NGP QM results seem to reproduce the experiments well, whereas the QCT method underestimates the amount of forward scattering by at least a factor of three. The comparison between experiment and theory has been performed by forward convolution of the theoretical results. Such a forward convolution involves a simulation of the time-of-flight profile that would be expected for a given theoretical center-of-mass differential cross section. The validity of this procedure for comparing the results of photoloc experiments with theory has already been assessed for HD($v' = 1, 2$) product-state-resolved DCSs (232). Because photoloc experiments measure directly a velocity distribution, the transformation between product laboratory speed and center-of-mass scattering angle implies a lower angular resolution to forward scattering and an increasing difficulty in separating the effects of height and width for narrow forward scattering peaks. Despite this limitation, both the experimental data and NGP QM calculations agree on the fact that the largest (total) amount of forward scattering relative to backward scattering occurs around 1.64 eV. We furthermore note that the crossed-beam experiments of Schnieder and coworkers have not been able to access the forward scattering region below 50° owing to geometrical constraints in the apparatus (backward-scattered D product is obscured by the presence of the reagent D_2 beam). From this quantitative comparison of experimental data and NGP QM calculations, it is possible to ascribe HD($v' = 3$, low-j') forward scattering (see Figure 4) to a primarily quantum-mechanical phenomenon also present in lower vibrational levels at lower collision energies. A partial-wave analysis of the QM calculations showed that a narrow range of high-J partial waves mainly caused the forward scattering. Based on the J-shifting approximation (58), it was possible to assign the strongest forward feature at 1.64 eV to the lowest bending level of the complex, a finding consistent with preferential decay into the rotationless product state HD($v' = 3$, $j' = 0$). By invoking the concept of vibrational adiabaticity, we can use the vibrational quantum label of the HD product to assign the symmetric stretch motion of the HD_2 complex to $v_1 = 3$. This full assignment of the quantum numbers of the HD_2 complex agrees with what Truhlar and coworkers (234) found.

Kendrick (109) has carried out further theoretical analyses of forward scattering in the $H + D_2$ reaction using converged NGP QM calculations. The appearance of forward-scattering features as a function of J led Kendrick to the general conclusion that it is unlikely that this feature can be interpreted as arising from resonances owing to the presence of significant classical and quantum mechanical nonresonant contributions at these scattering angles. These conclusions do not agree with NGP QM (F.J. Aoiz, L. Bañares, J.F. Castillo, B.D. Bean, F. Fernández-Alonso, et al., unpublished results) and QCT (110) results that indicate a relatively narrow contribution of partial waves to forward scattering as well as a marked difference between QCT and QM results. Furthermore, we note that the experimental data meet the two requirements needed to fulfill the operational definition of scattering resonances (see Introduction), namely: (*a*) the amount of HD($v' = 3$, j') forward scattering varies rapidly with collision energy and product rotational excitation; and (*b*) reactive flux leading to forward-scattering features has been associated with metastability of the triatomic complex. It is still unclear from a theoretical viewpoint whether

the trapping of the system in the transition-state region is caused by one or more conventional resonances or by the presence of a threshold effect (see Sections 2.2 and 2.3). An explanation along the latter lines would necessarily need to account for the preferential decay into HD($v' = 3$, $j' = 0$) and, to a lesser extent, into HD($v' = 3$, $j' = 1$) observed in the experiments. We once more note that whether threshold effects may be considered scattering resonances in their own right is still a matter of discussion in the chemical physics community. It is beyond the scope of this review to provide an answer to this pending yet important question. Of course, identifying resonance features either in the laboratory or by accurate quantum mechanical calculations is very different from understanding what causes them.

Recently, Althorpe (220) has made a breakthrough in being able to perform full scattering calculations using time-dependent wave packet propagation methods for the H + H_2 reaction family. This approach is considerably faster than time-independent methods and will probably find its best use in more complex reaction systems. Figure 7 shows a series of time-elapsed snapshots of the H + $D_2 \rightarrow$ HD($v' = 3$, $j' = 0$) + D reaction over an energy range of 0.9–2.4 eV (S.C. Althorpe, unpublished results). This "movie" shows that the amount of forward-scattered HD($v' = 3$, $j' = 0$) product constitutes a considerable fraction of the overall flux. Moreover, the forward-scattered component lags the backward-scattered component by about 25 fs owing to temporary trapping in the transition-state region. The major features shown in Figure 7 are in qualitative agreement with previous QCT results and indicate a very different and more indirect underlying mechanism leading to forward scattering. A detailed analysis of these very interesting theoretical results, however, needs to be completed before we can fully understand what causes the observed resonance features.

The product of HD($v' = 3$, $j' = 0$) is truly a small fraction of the product yield. Specifically, it is estimated to have a total cross section of $\sim 10^{-3}$ Å^2 whereas the total reaction cross section is on the order of ~ 1 Å^2. Most scattering is direct and can be simply described using billiard-ball models. Nevertheless, it is remarkable how much detailed information can be gained from a study of the tiny fraction of the overall cross section showing signatures ascribable to reactive scattering resonances.

4. BEYOND STATE-RESOLVED DIFFERENTIAL CROSS SECTIONS

4.1. Vector Correlations in Scattering Experiments

What is to be measured beyond state-, energy-, and angle-resolved cross sections? If we think in terms of the vector properties or stereodynamics of a chemical reaction, a DCS constitutes what is called a two-vector (k-k′) correlation: it relates the relative direction of reagents (k) to that of products (k′). Other vector correlations are possible, as for example, k-j′ (where j′ is the rotational angular momentum vector of the product), k-k′-j′, etc. For more details about vector properties in photodissociation and chemical reactions, the reader is referred to the original

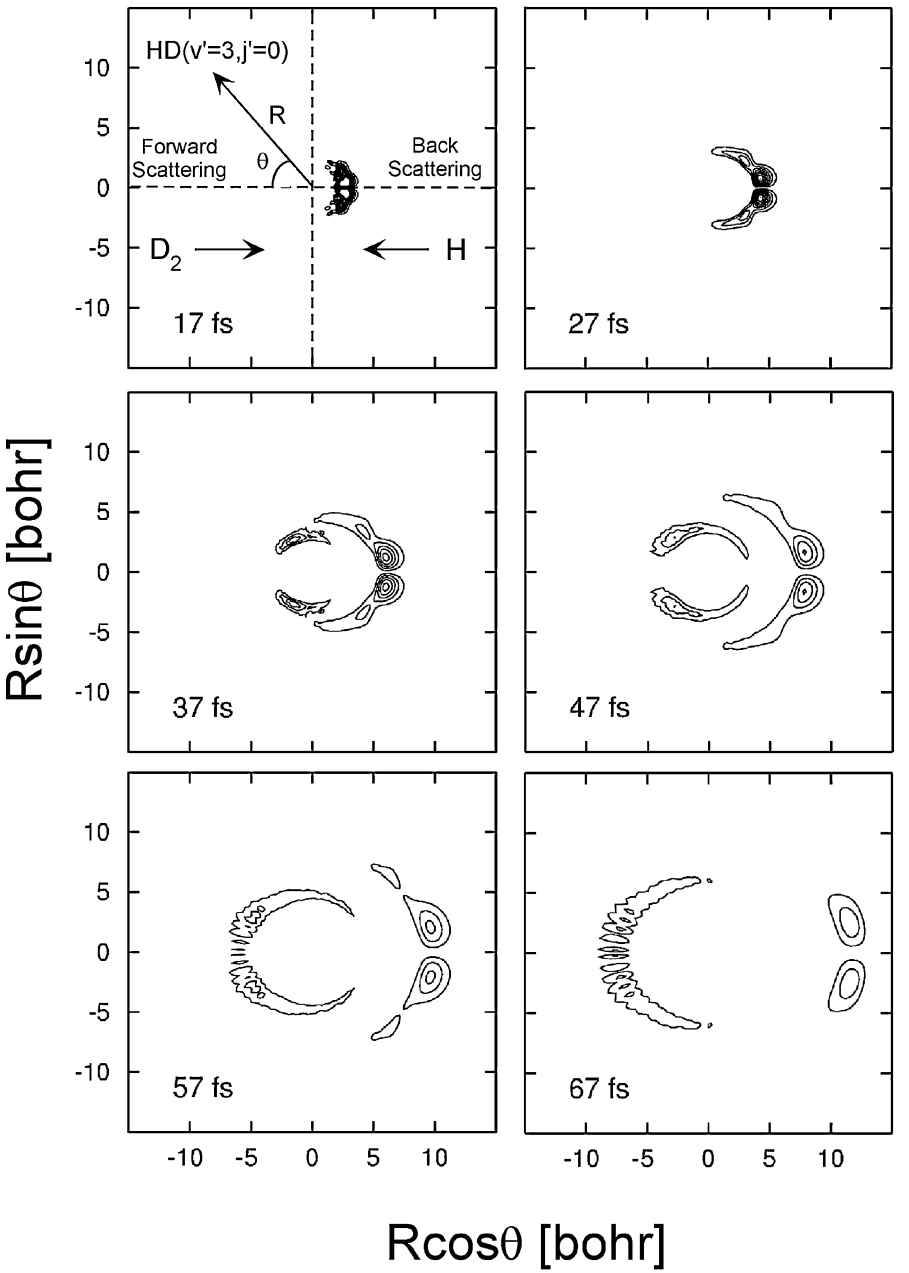

Figure 7 Wave packet snapshots of the reaction H + D_2(v = 0, j = 0) → HD(v′ = 3; j′ = 0) + D over a total energy range of 0.9–2.4 eV as calculated by a time-dependent method (see text for details) and starting at an H-D_2 separation of 6 bohr. The first snapshot, at a time of 17 fs, shows the directions of the incoming reagents and outgoing HD(v′ = 3, j′ = 0) products.

papers (237), several reviews (238–242), devoted journal volumes (243, 244), and more recent work not yet reviewed (114, 245–248). The stereodynamics of a few chemical reactions, including Cl + HD (249), Cl + CH_4 (250, 251), and Cl + C_2H_6 (252–255), have been studied using the photoloc technique by Zare and coworkers. In these experiments, state-selective detection of HCl, CH_3, and C_2H_5 molecules allows for a simultaneous measurement of the angle-resolved spatial distribution of product angular momenta. In addition, SRP techniques have also permitted the study of k-j-k′ correlations for vibrationally excited reagents, which can be readily associated with the steric requirements of a chemical reaction. Kandel et al. (249) have used the SRP technique to study the stereochemistry of the Cl + HD($v = 1$; $j = 1, 2$) reaction.

As for the H + H_2 reaction, work along similar lines has been mainly hampered by the lack of suitable multiphoton detection schemes sensitive to the angular momentum anisotropy. Recently, Zare and coworkers (256) have developed a novel multiphoton ionization detection scheme for the H_2 molecule that may prove useful in future investigations of product polarization in the hydrogen exchange reaction. Such progress on the experimental side has been also complemented by recent classical and quantal descriptions of the stererodynamics of elementary chemical reactions by de Miranda et al. (257). The benchmark system used in this work has been the prototypical H + D_2 reaction at a collision energy of 1.29 eV. It was shown that a study of the vector correlations would deepen significantly our knowledge about the PES and reaction mechanisms. The search for resonance features using these novel tools is not an exception to these conclusions as evidenced, for example, by the magnetic-sublevel-resolved QM DCS calculated by Miller & Zhang for the H + H_2 and D + H_2 reactions (83). Moreover, the study of stereodynamical effects offers the experimentalist additional means of investigating dynamical features that other and more highly averaged observables may tend to obscure.

As for the use of experimental techniques to prepare reagents with an anisotropic spatial distribution, SRP techniques are mandatory for homonuclear diatomics like H_2 and isotopologs. There has been some work in this direction for ICS measurements in D + H_2 (81, 222–224) and H + D_2 (258) but not for state-resolved angular distributions. Given the propensity for the H + H_2 reaction to be collinear, we would expect significant changes in the angular distributions as the reagent relative velocity vector is preferentially aligned parallel or perpendicular to the diatom bond axis. If our current picture of quasibound states in the H + D_2 reaction leading to forward scattering features is to stand the test of time, these experiments will undoubtedly be extremely insightful.

4.2. Direct Observation of the H_3 Transition-State Region: Electron Attachment/Detachment Experiments

An ever-present concern in this review was related to the effect of partial-wave summation over the outcome of asymptotic reactive scattering experiments. This necessary evil in collision experiments has hampered the unambiguous detection

of quasibound states in reactive scattering. Experimentally, several ways exist to avoid this averaging process. The central idea is based on the preparation of a stable precursor, for example, the positive or negative ion of the compound species of interest. Either light to photodetach a negative ion or charge neutralization in the case of the positive ion may be used to launch almost instantaneously the stable precursor onto the transition-state region of a chemical reaction. Examples of this approach are the famous photodetachment experiments of Neumark and coworkers on the transition state spectroscopy of various triatoms including FH_2 and IHI (259). This unconventional way of probing the transition state region has given strong evidence for the existence of transition-state resonances in the IHI system.

At the moment, all experiments on the dissociation of H_3 states use the H_3^+ ion as precursor. Charge neutralization in alkali-metal vapors leads to two- and three-body breakup of the triatomic complex [see, for example, Krause et al. (260) for an early quantum mechanical treatment and simulation of experiments]. The UV spectra of H_3, D_2H, and H_2D have been studied using both experimental and theoretical methods (261–265). The bimodal structure observed in these spectra in the range of 200–400 nm has been interpreted as arising from radiative decay into the two Jahn-Teller sheets of the ground-state PES (also responsible for GP effects). Mahapatra & Köppel (265) have found in their time-dependent calculations distinct differences between resonance states associated with each adiabatic sheet, the upper one leading to a much more pronounced and more easily assigned structure.

Cold ion storage rings have also been used in the last decade to achieve relative collision energies for recombination as low as 0.001 eV (266–268). These experiments have measured recoil energy as well as angular distributions for two- and three-body breakup, but they still lack product-state selectivity. Very recently, Kokoouline et al. (269) have made significant progress in the theoretical understanding of the recombination of H_3^+ by electron impact at low energies (<1 eV). In their theoretical treatment, it is mandatory to incorporate the Jahn-Teller-symmetry-distortion effect in order to explain the large dissociation recombination rates, the $(H + H + H)/(H_2 + H)$ branching fraction, and the vibrational distribution of H_2 products already measured using cold ion storage rings. In addition, H_3 excited states can be sufficiently long-lived to allow initial-state selection by laser pumping. Helm, Müller, and coworkers have embarked on a detailed characterization of the fragmentation dynamics of state-selected Rydberg H_3 states into $H + H + H$ (270–272) and $H + H_2(v', j')$ (273, 274), and they are at a point to achieve product-state resolution in very impressive and technically involved two- and three-particle coincidence experiments.

Photodetachment experiments akin to the ones pioneered by Neumark and coworkers are also possible for the H_3 triatomic system. As early as 1975, Aberth, Schnitzer, & Anbar (275) performed the mass-spectrometric detection of H_3^-, H_2D^-, HD_2^-, and D_3^- anions using a hollow-cathode duoplasmatron negative-ion source. The half-lives for these triatomic species were estimated to be greater than 10 μs. Sadeghi & Skodje (140) have noted that Franck-Condon overlaps between the negative and neutral species will be significant for vibrationally excited H_3^- and

will make possible experiments that can be compared against their time-dependent wave packet calculations (140–143).

CONCLUDING REMARKS

Resonances are exquisitely sensitive probes of the nature of the scattering process. It is for the simplest of chemical reactions, the $H + H_2$ reaction family, that we expect theory to be most advanced. These reactions are not simple from an experimental viewpoint. Nevertheless, experiments have reached a level of sophistication that makes possible the observation of resonance features in spite of the overwhelming dominance of direct dynamics. Both theory and experiment are needed. It is not enough to measure only scattering features. It is also not enough to calculate them. What is needed is to develop simple pictures and accurate approximations that can be transferred to other reactions that display a richer chemistry.

ACKNOWLEDGMENTS

This work was supported at Stanford University by the U.S. National Science Foundation under grant number CHE-99-00305. F.F.A. acknowledges financial support in the form of a Marie Curie Fellowship of the European Program "Improving Human Research Potential and the Socioeconomic Knowledge Base" under contract number HPMFCT-2000-00683. We thank our coworkers B.D. Bean, J.D. Ayers, and A.E. Pomerantz for their contribution to the experimental work carried out at Stanford University as well as for useful discussions and suggestions. We also thank F.J. Aoiz, L. Bañares, J.F. Castillo, and S.C. Althorpe for sharing the results of their calculations prior to publication.

LITERATURE CITED

1. Condon EU, Shortley GH. 1977. *The Theory of Atomic Spectra*. New York: Cambridge Univ. Press
2. Graybeal JD. 1988. *Molecular Spectroscopy*. New York: McGraw-Hill
3. Fermi E. 1934. *Nature* 133:757
4. Fermi E. 1934. *Nature* 133:898–99
5. Fermi E, Amaldi E, D'Agostino O, Rasetti F, Segré E. 1934. *Proc. R. Soc. London Ser. A* 133:483–500
6. Amaldi E, D'Agostino O, Fermi E, Pontecorvo B, Rasetti F, Segré E. 1935. *Proc. R. Soc. London Ser. A* 149:522–58
7. Bethe HA. 1935. *Phys. Rev.* 47:747–59
8. Bohr N. 1936. *Nature* 137:344–48
9. Breit G, Wigner EP. 1936. *Phys. Rev.* 49: 519–31
10. Fano U. 1961. *Phys. Rev.* 124:1866–78
11. Frauenfelder H, Henley EM. 1974. *Subatomic Physics*. Englewood Cliffs, NJ: Prentice-Hall
12. Blatt JM, Weisskopf VF. 1979. *Theoretical Nuclear Physics*. New York: Springer
13. Feshbach H. 1992. *Theoretical Nuclear Physics: Nuclear Reactions*. New York: Wiley
14. Burke PG. 1968. *Adv. At. Mol. Phys.* 4: 173–19

15. Golden DE. 1978. *Adv. At. Mol. Phys.* 14:1–85
16. Auger P. 1925. *J. Phys. Radium* 6:205–8
17. Haas R. 1957. *Z. Phys.* 148:177–91
18. Schulz GJ. 1959. *Phys. Rev.* 116:1141–47
19. Herzenberg A, Mandl F. 1962. *Proc. R. Soc. London Ser. A* 270:48–71
20. Schulz GJ, Fox RE. 1957. *Phys. Rev.* 106: 1179–81
21. Baranger E, Gerjouy E. 1957. *Phys. Rev.* 106:1182–85
22. Phelps AV. 1968. *Rev. Mod. Phys.* 40:399–410
23. Schulz GJ. 1973. *Rev. Mod. Phys.* 45:378–422
24. Schulz GJ. 1973. *Rev. Mod. Phys.* 45:423–86
25. Biondi MA, Herzenberg A, Kuyatt CE. 1979. *Phys. Today* 32:44–49
26. Morrison MA. 1987. *Adv. At. Mol. Phys.* 24:51–56
27. Buckman SJ, Clark CW. 1994. *Rev. Mod. Phys.* 66:539–655
28. Patel CKN. 1964. *Phys. Rev. Lett.* 13:617–19
29. Cheo PK. 1971. In *Lasers, A Series of Advances*, ed. AK Levine, AJ DeMaria, pp. 111–267. New York: Marcel Dekker
30. Boudaïffa B, Cloutier P, Hunting D, Huels MA, Sanche L. 2000. *Science* 287: 1658–60

30a. Eu BC, Ross J. 1966. *J. Chem. Phys.* 44: 2467–75
30b. Levine RD. 1967. *J. Chem. Phys.* 46:331–45
30c. Micha DA. 1967. *Chem. Phys. Lett.* 1: 139–42
30d. Micha DA. 1967. *Phys. Rev.* 162:88–97
30e. O'Malley TF. 1967. *Phys. Rev.* 162:98–104
30f. Levine RD. 1968. *J. Chem. Phys.* 49:51–55
30g. Levine RD, Johnson BR, Muckerman JT, Bernstein RB. 1968. *Chem. Phys. Lett.* 1:517–20
30h. Levine RD, Johnson BR, Muckerman JT, Bernstein RB. 1968. *J. Chem. Phys.* 49: 56–64
30i. Johnson BR, Shapiro M, Levine RD. 1969. *Chem. Phys. Lett.* 3:131–33
30j. Levine RD. 1970. *Acc. Chem. Res.* 3:273–80
30k. Secrest D. 1973. *Annu. Rev. Phys. Chem.* 24:379–406
30l. Miller WH. 1970. *J. Chem. Phys.* 52:543–51
30m. Miller WB, Safron SA, Herschbach DR. 1967. *Faraday Discuss. Chem. Soc.* 44: 108–22

31. Truhlar DG, Kuppermann A. 1970. *J. Chem. Phys.* 52:3841–43
32. Truhlar DG, Kuppermann A. 1972. *J. Chem. Phys.* 56:2232–52
33. Levine RD, Wu S-F. 1971. *Chem. Phys. Lett.* 11:557–61
34. Hirschfelder JO, Eyring H, Topley B. 1936. *J. Chem. Phys.* 4:170–77
35. London F. 1929. *Z. Elektrochem.* 35:552–55
36. Ering H, Polanyi M. 1931. *Z. Phys. Chem. Abt. B* 12:279–311
37. Porter RN, Karplus M. 1964. *J. Chem. Phys.* 40:1105–15
38. Shavitt I, Stevens RM, Minn FL, Karplus M. 1968. *J. Chem. Phys.* 48:2700–13
39. Truhlar DG, Wyatt RE. 1977. *Adv. Chem. Phys.* 36:141–204
40. Wu S-F, Levine RD. 1971. *Mol. Phys.* 22:881–97
41. Wu S-F, Johnson BR, Levine RD. 1973. *Mol. Phys.* 25:609–30
42. Wu S-F, Johnson BR, Levine RD. 1973. *Mol. Phys.* 25:839–56
43. Schatz GC, Kuppermann A. 1973. *J. Chem. Phys.* 59:964–65
44. Feshbach H. 1958. *Ann. Phys.* 5:357–90
45. Feshbach H. 1962. *Ann. Phys.* 19:287–313

45a. Feshbach H. 1967. *Ann. Phys.* 43:410–20

46. Schatz GC, Kuppermann A. 1975. *Phys. Rev. Lett.* 35:1266–69
47. Truhlar DG, Wyatt RE. 1976. *Annu. Rev. Phys. Chem.* 47:1–43
48. Kuppermann A. 1981. In *Potential Energy Surfaces and Dynamics Calculations*, ed.

DG Truhlar, pp. 375–420. New York: Plenum
49. Garrett BC, Truhlar DG. 1982. *J. Phys. Chem.* 86:1136–41
50. Garrett BC, Schwenke DW, Skodje RT, Thirumalai D, Thompson TC, Truhlar DG. 1984. In *Resonances in Electron-Molecule Scattering, Van der Waals Complexes, and Reactive Chemical Dynamics. ACS Symp. Ser.*, ed. DG Truhlar, pp. 375–400. Washington, DC: ACS
51. Kuppermann A, Kaye JA, Dwyer JP. 1980. *Chem. Phys. Lett.* 74:257–62
52. Launay JM, LeDourneuf M. 1982. *J. Phys. B: At. Mol. Phys.* 15:L455–61
53. Römelt J. 1983. *Chem. Phys.* 79:197–209
54. Marston CC, Wyatt RE. 1984. *Chem. Phys.* 81:1819–24
55. Pollak E, Wyatt RE. 1984. *J. Chem. Phys.* 81:1801–12
56. Bowman JM. 1986. *Chem. Phys. Lett.* 124:260–63
57. Bowman JM. 1985. *Adv. Chem. Phys.* 61: 115–63
58. Bowman JM. 1991. *J. Phys. Chem.* 95: 4960–68
59. Child MS, Pollak E. 1980. *J. Chem. Phys.* 73:4365–72
60. Pollak E, Child MS. 1980. *J. Chem. Phys.* 73:4373–80
61. Pollak E, Child MS, Pechukas P. 1980. *J. Chem. Phys.* 72:1669–78
62. Pollak E. 1981. *J. Chem. Phys.* 74:5586–94
63. Pollak E, Wyatt RE. 1983. *J. Chem. Phys.* 78:4464–76
64. Pollak E, Child MS. 1981. *Chem. Phys.* 60:23–32
65. Manz J, Pollak E, Römelt J. 1982. *Chem. Phys. Lett.* 86:26–32
66. Pollak E, Wyatt RE. 1982. *J. Chem. Phys.* 77:2689–91
67. Pollak E. 1987. *Chem. Phys. Lett.* 137: 171–74
68. Hipes PG, Kuppermann A. 1987. *Chem. Phys. Lett.* 133:1–7
69. Nieh J-C, Valentini JJ. 1988. *Phys. Rev. Lett.* 60:519–22
70. Nieh J-C, Valentini JJ. 1990. *J. Chem. Phys.* 92:1083–97
71. Phillips DL, Levene HB, Valentini JJ. 1989. *J. Chem. Phys.* 90:1600–9
72. Buchenau H, Toennies JP, Arnold J, Wolfrum J. 1990. *Ber. Bunsenges. Phys. Chem.* 94:1231–48
73. Colton MC, Schatz GC. 1986. *Chem. Phys. Lett.* 124:256–59
74. Schatz GC. 1988. *Annu. Rev. Phys. Chem.* 39:317–40
75. Webster F, Light JC. 1986. *J. Chem. Phys.* 85:4744–55
76. Zhang JZH, Miller WH. 1988. *Chem. Phys. Lett.* 153:465–70
77. Zhang JZH, Miller WH. 1989. *Chem. Phys. Lett.* 159:130–33
78. Zhang JZH, Miller WH. 1989. *J. Chem. Phys.* 91:1528–47
79. Manolopoulos DE, Wyatt RE. 1989. *Chem. Phys. Lett.* 159:123–29
80. Launay JM, LeDourneuf M. 1989. *Chem. Phys. Lett.* 163:178–88
81. Kliner DAV, Adelman DE, Zare RN. 1991. *J. Chem. Phys.* 94:1069–80
82. Miller WH. 1990. *Annu. Rev. Phys. Chem.* 41:245–81
83. Miller WH, Zhang JZH. 1991. *J. Phys. Chem.* 95:12–19
84. Aoiz FJ, Herrero VJ, Rábanos VS. 1991. *J. Chem. Phys.* 95:7767–68
85. Aoiz FJ, Herrero VJ, Rábanos VS. 1994. *J. Chem. Phys.* 97:7423–36
86. Aoiz FJ, Bañares L, Herrero VJ. 1998. *Adv. Class. Trajectory Methods* 3:121–82
87. Siegbahn P, Liu B. 1978. *J. Chem. Phys.* 68:2457–65
88. Truhlar DG, Horowitz CJ. 1978. *J. Chem. Phys.* 68:2466–76
89. Truhlar DG, Horowitz CJ. 1979. *J. Chem. Phys.* 71:1514
90. Varandas AJC, Brown FB, Mead CA, Truhlar DG, Blais NC. 1987. *J. Chem. Phys.* 86:6258–69
91. Boothroyd AI, Keogh WJ, Martin PG, Peterson MR. 1991. *J. Chem. Phys.* 95: 4343–59

92. Boothroyd AI, Keogh WJ, Martin PG, Peterson MR. 1996. *J. Chem. Phys.* 104: 7139–52
93. Wu Y-SM, Kuppermann A, Anderson JB. 1999. *Phys. Chem. Chem. Phys.* 1:929–37
94. Skodje RT, Skouteris D, Manolopoulos DE, Lee S-H, Dong F, Liu K. 2000. *J. Chem. Phys.* 112:4536–52
95. Skodje RT, Skouteris D, Manolopoulos DE, Lee S-H, Dong F, Liu K. 2000. *Phys. Rev. Lett.* 85:1206–9
96. Schatz GC. 2000. *Science* 288:1599–600
97. Liu K. 2001. *Annu. Rev. Phys. Chem.* 52:139–64
98. Dong F, Lee S-H, Liu K. 2000. *J. Chem. Phys.* 113:3633–40
99. Chao SD, Skodje RT. 2000. *J. Chem. Phys.* 113:3487–91
100. Sokolovski D, Castillo JF. 2000. *Phys. Chem. Chem. Phys.* 2:507–12
101. Castillo JF, Manolopoulos DE, Stark K, Werner H-J. 1996. *J. Chem. Phys.* 104:6531–46
102. Neumark DM, Wodtke AM, Robinson GN, Hayden CC, Lee YT. 1985. *J. Chem. Phys.* 82:3045–66
103. Neumark DM, Wodtke AM, Robinson GN, Hayden CC, Shobatake K, et al. 1985. *J. Chem. Phys.* 82:3045–66
104. Wrede E, Schnieder L. 1997. *J. Chem. Phys.* 107:786–90
105. Kendrick BK, Jayasinghe L, Moser S, Auzinsh M, Shafer-Ray N. 2000. *Phys. Rev. Lett.* 84:432–58
106. Kendrick BK, Jayasinghe L, Moser S, Auzinsh M, Shafer-Ray N. 2001. *Phys. Rev. Lett.* 86:2482
107. Chao SD, Skodje RT. 2001. *Chem. Phys. Lett.* 336:364–70
108. Aoiz FJ, Bañares L, Castillo JF. 2001. *J. Chem. Phys.* 114:823–79
109. Kendrick BK. 2001. *J. Chem. Phys.* 114: 8796–819
110. Fernández-Alonso F, Bean BD, Ayers JD, Pomerantz AE, Zare RN, et al. 2000. *Angew. Chem. Int. Ed.* 39:2748–52
111. Bean BD. 2000. *The hydrogen atom, hydrogen molecule exchange reaction. Experimental evidence for dynamical resonances in chemical reactions*. PhD thesis. Stanford Univ. 106 pp.
112. Deleted in proof
113. Shafer NE, Orr-Ewing AJ, Simpson WR, Xu H, Zare RN. 1993. *Chem. Phys. Lett.* 212:155–62
114. Shafer-Ray NE, Orr-Ewing AJ, Zare RN. 1995. *J. Phys. Chem.* 99:7591–603
115. Marcus RA. 1966. *J. Chem. Phys.* 45: 4493–99
116. Marcus RA. 1966. *J. Chem. Phys.* 45: 4500–4
117. Levine RD. 1969. *Quantum Mechanics of Molecular Rate Processes*. Oxford: Oxford Univ. Press
118. Light JC. 1970. *Adv. Chem. Phys.* 19:1–31
119. Child MS. 1974. *Molecular Collision Theory*. London/New York: Academic
120. Levine RD, Bernstein RB. 1987. *Molecular Reaction Dynamics and Chemical Reactivity*. Oxford: Oxford Univ. Press
121. Chapman FM, Hayes EF. 1975. *J. Chem. Phys.* 62:4400–3
122. Chapman FM, Hayes EF. 1976. *J. Chem. Phys.* 65:1032–33
123. Aquilanti V, Capecchi G, Cavalli S, Fazio DD, Palmieri P, et al. 2000. *Chem. Phys. Lett.* 318:619–28
124. Newton RG. 1982. *Scattering Theory of Waves and Particles*. Heidelberg: Springer-Verlag
125. Taylor JR. 1972. *Scattering Theory*. New York: Wiley
126. Smith FT. 1960. *Phys. Rev.* 118:349–56
127. Simons JP. 1997. *J. Chem. Soc. Faraday Trans.* 93:4095–105
128. Green WH, Moore CB, Polik WF. 1992. *Annu. Rev. Phys. Chem.* 43:591–626
129. Reid SA, Reisler H. 1996. *Annu. Rev. Phys. Chem.* 47:495–525
130. Friedman RS, Truhlar DG. 1991. *Chem. Phys. Lett.* 183:539–46
131. Eckart C. 1930. *Phys. Rev.* 35:1303–9
132. Friedman RS, Hullinger VD, Truhlar DG. 1995. *J. Phys. Chem.* 99:3184–94
133. Seideman T, Miller WH. 1991. *J. Chem. Phys.* 95:1768–80

134. Ryabov V, Moiseyev N. 1993. *J. Chem. Phys.* 98:9618–23
135. Siegert AJF. 1939. *Phys. Rev.* 56:750–52
136. Bohm A. 1986. *Quantum Mechanics: Foundations and Applications*. New York: Springer-Verlag
137. Junker BR. 1982. *Adv. At. Mol. Phys.* 18:207–63
138. Atabek O, Lefebvre R, Sucre MG, Gomez-Llorente J, Taylor H. 1991. *Int. J. Quant. Chem.* 40:211–24
139. Landau LD, Lifshitz EM. 1977. *Quantum Mechanics* (*Non-relativistic Theory*). New York: Pergamon
140. Sadeghi R, Skodje RT. 1993. *J. Chem. Phys.* 98:9208–10
141. Sadeghi R, Skodje RT. 1993. *J. Chem. Phys.* 99:5126–40
142. Skodje RT, Sadeghi R, Köppel H, Krause JL. 1994. *J. Chem. Phys.* 101:1725–29
143. Sadeghi R, Skodje RT. 1995. *J. Chem. Phys.* 102:193–213
144. Sadeghi R, Skodje RT. 1995. *Phys. Rev. A* 52:1996–2010
145. Varandas AJC, Yu HG. 1996. *Chem. Phys. Lett.* 259:336–41
146. Varandas AJC, Yu HG. 1996. *Chem. Phys.* 209:31–40
147. Yu HG, Varandas AJC. 1996. *J. Phys. Chem.* 100:14598–601
148. Varandas AJC, Yu HG. 1999. *J. Mol. Struct. Theochem.* 493:81–88
149. Manz J, Meyer R, Pollak E, Römelt J. 1982. *Chem. Phys. Lett.* 93:184–87
150. Manz J, Meyer R, Römelt J. 1983. *Chem. Phys. Lett.* 96:607–12
151. Clary DC, Connor JNL. 1983. *Chem. Phys. Lett.* 94:81–84
152. Pollak E. 1983. *Chem. Phys. Lett.* 94:85–89
153. Pollak E. 1983. *J. Chem. Phys.* 78:1228–36
154. Atabek O, Lefebvre R. 1983. *Chem. Phys. Lett.* 98:559–62
155. Clary DC, Connor JNL. 1984. *J. Phys. Chem.* 88:2758–64
156. Manz J, Meyer R, Pollak E, Römelt J, Schor HHR. 1984. *Chem. Phys.* 83:333–43
157. Garrett BC, Lynch GC, Allison TC, Truhlar DG. 1998. *Comp. Phys. Commun.* 109:47–54
158. Truhlar DG, Garrett BC. 1992. *J. Phys. Chem.* 96:6515–18
159. Chatfield DC, Friedman RS, Mielke SL, Lynch GC, Allison TC, et al. 1996. In *Dynamics of Molecules and Chemical Reactions*, ed. RE Wyatt, JZH Zhang, pp. 323–86. New York: Marcel Dekker
160. Truhlar DG, Garrett BC, Klippenstein SJ. 1996. *J. Phys. Chem.* 100:12771–800
161. Chatfield DC, Friedman RS, Truhlar DG, Garrett BC, Schwenke DW. 1991. *J. Am. Chem. Soc.* 113:486–94
162. Chatfield DC, Friedman RS, Truhlar DG. 1991. *Faraday Discuss. Chem. Soc.* 91: 289–304
163. Truhlar DG. 1991. *Faraday Discuss. Chem. Soc.* 91:395–98
164. Chatfield DC, Truhlar DG, Schwenke DW. 1992. *J. Chem. Phys.* 96:4313–23
165. Chatfield DC, Friedman RS, Schwenke DW, Truhlar DG. 1992. *J. Phys. Chem.* 96:2414–21
166. Chatfield DC, Mielke SL, Allison TC, Truhlar DG. 2000. *J. Chem. Phys.* 112: 8387–408
167. Lynch GC, Halvick P, Zhao M, Truhlar DG, Yu C-h, et al. 1991. *J. Chem. Phys.* 94:7150–58
168. Kress JD, Hayes EF. 1992. *J. Chem. Phys.* 97:4881–89
169. Bowman JM. 1987. *Chem. Phys. Lett.* 141:545–47
170. Haug K, Schwenke DW, Truhlar DG, Zhang Y, Zhang JZH, Kouri DJ. 1987. *J. Chem. Phys.* 87:1892–94
171. Chatfield DC, Friedman RS, Lynch GC, Truhlar DG. 1993. *J. Chem. Phys.* 98:342–62
172. Pack RT, Butcher EA, Parker GT. 1993. *J. Chem. Phys.* 99:9310–13
173. Leforestier C, Miller WH. 1994. *J. Chem. Phys.* 100:733–35

174. Zhang DH, Zhang JZH. 1994. *J. Chem. Phys.* 101:3671–78
175. Chatfield DC, Friedman RS, Lynch GC, Truhlar DG. 1992. *J. Phys. Chem.* 96:57–63
176. Srinivasan J, Allison TC, Schwenke DW, Truhlar DG. 1999. *J. Phys. Chem. A* 103:1487–503
177. Darakjian Z, Hayes EF, Parker GA, Butcher EA, Kress JD. 1991. *J. Chem. Phys.* 95:2516–22
178. Klippenstein SJ, Kress JD. 1992. *J. Chem. Phys.* 96:8164–70
179. Kress JD. 1991. *J. Chem. Phys.* 95:8673–74
180. Kress JD, Walker RB, Hayes EF, Pendergast P. 1994. *J. Chem. Phys.* 100:2728–42
181. Cuccaro SA, Hipes PG, Kuppermann A. 1989. *Chem. Phys. Lett.* 157:440–46
182. Zhao M, Mladenovic M, Truhlar DG, Schwenke DW, Sharafeddin O, et al. 1989. *J. Chem. Phys.* 91:5302–9
183. Zhao M, Rice SA. 1994. *J. Phys. Chem.* 98:3444–49
184. Schnieder L, Meier W, Welge KH, Ashfold MNR, Western CM. 1990. *J. Chem. Phys.* 92:7027–37
185. Merkt F, Xu H, Zare RN. 1996. *J. Chem. Phys.* 104:950–61
186. Rinnen K-D, Kliner DAV, Zare RN, Huo WM. 1989. *Isr. J. Chem.* 29:369–82
187. Huo WM, Rinnen K-D, Zare RN. 1991. *J. Chem. Phys.* 95:205–13
188. Rinnen K-D, Buntine MA, Kliner DAV, Zare RN, Huo WM. 1991. *J. Chem. Phys.* 95:214–25
189. D'Mello M, Manolopoulos DE, Wyatt RE. 1991. *J. Chem. Phys.* 94:5985–93
190. Rinnen K, Kliner D, Zare RN. 1989. *J. Chem. Phys.* 91:7514–29
191. Zhao M, Truhlar DG, Blais NC, Schwenke DW, Kouri DJ. 1990. *J. Phys. Chem.* 94:6696–706
192. Webster F, Light JC. 1989. *J. Chem. Phys.* 90:300–21
193. Yarkony DR. 1996. *Rev. Mod. Phys.* 68: 985–1013
194. Mead CA. 1992. *Rev. Mod. Phys.* 64:51–85
195. Lepetit B, Kuppermann A. 1990. *Chem. Phys. Lett.* 166:581–88
196. Wu Y-SM, Kuppermann A, Lepetit B. 1991. *Chem. Phys. Lett.* 186:319–28
197. Wu Y-SM, Kuppermann A. 1993. *Chem. Phys. Lett.* 201:178–86
198. Kuppermann A, Wu Y-SM. 1993. *Chem. Phys. Lett.* 205:577–36
199. Kuppermann A, Wu Y-SM. 1995. *Chem. Phys. Lett.* 241:229–40
200. Wu Y-SM, Kuppermann A. 1995. *Chem. Phys. Lett.* 235:105–10
201. Baer M. 2000. *Chem. Phys.* 259:123–47
202. Yarkony DR. 2001. *J. Phys. Chem. A* 105:6277–93
203. Mordaunt DH, Ashfold MN, Dixon RN. 1996. *J. Chem. Phys.* 104:6460–71
204. Mordaunt DH, Dixon RN, Ashfold MN. 1996. *J. Chem. Phys.* 104:6472–81
205. Dixon RN. 1996. *Mol. Phys.* 88:949–77
206. Mordaunt DH, Ashfold MN, Dixon RN. 1998. *J. Chem. Phys.* 109:7659–62
207. Casavecchia P, Balucani N, Volpi GG. 1999. *Annu. Rev. Phys. Chem.* 50:347–76
208. Casavecchia P. 2000. *Rep. Prog. Phys.* 63:355–414
209. Schnieder L, Seekamp-Rahn K, Wrede E, Welge KH. 1997. *J. Chem. Phys.* 107: 6175–95
210. Bañares L, Aoiz FJ, Herrero VJ, D'Mello MJ, Niederjohann B, et al. 1998. *J. Chem. Phys.* 108:6160–69
211. Schnieder L, Seekamp-Rahn K, Borkowski J, Wrede E, Welge KH, et al. 1995. *Science* 269:207–10
212. Wrede E, Schnieder L, Welge KH, Aoiz FJ, Bañares L, Herrero VJ. 1997. *Chem. Phys. Lett.* 265:129–36
213. Wrede E, Schnieder L, Welge KH, Aoiz FJ, Bañares L, et al. 1999. *J. Chem. Phys.* 110:9971–81
214. Wrede E, Schnieder L, Welge KH, Aoiz FJ, Bañares L, et al. 1997. *J. Chem. Phys.* 106:7862–64
215. Kendrick BK. 2000. *J. Chem. Phys.* 112: 5679–704

216. Kendrick BK. 2001. *J. Chem. Phys.* 114: 4335–42
217. Xu ZR, Varandas AJC. 2001. *J. Phys. Chem. A* 105:2246–50
218. Mahapatra S, Köppel H, Cederbaum LS. 2001. *J. Phys. Chem. A* 105:2321–29
219. Kliner DAV, Adelman DE, Zare RN. 1991. *J. Chem. Phys.* 95:1648–62
220. Althorpe SC. 2001. *J. Chem. Phys.* 114: 1601–16
221. Farrow RL, Chandler DW. 1988. *J. Chem. Phys.* 89:1994–98
222. Adelman DE, Shafer NE, Kliner DAV, Zare RN. 1992. *J. Chem. Phys.* 97:7323–41
223. Kliner DAV, Zare RN. 1990. *J. Chem. Phys.* 92:2107–9
224. Neuhauser D, Judson RS, Kouri DJ, Adelman DE, Shafer NE, et al. 1992. *Science* 257:519–22
225. Gostein M, Parhikhteh H, Sitz GO. 1995. *Phys. Rev. Lett.* 75:342–45
226. Gostein M, Watts E, Sitz GO. 1997. *Phys. Rev. Lett.* 79:2891–94
227. Shafer NE, Xu H, Tuckett RP, Springer M, Zare RN. 1993. *J. Phys. Chem.* 98: 3369–78
228. Fernández-Alonso F, Bean BD, Zare RN. 1999. *J. Chem. Phys.* 111:1022–34
229. Simpson WR, Orr-Ewing AJ, Rakitzis TP, Kandel SA, Zare RN. 1995. *J. Chem. Phys.* 103:7299–312
230. Fernández-Alonso F, Bean BD, Zare RN. 1999. *J. Chem. Phys.* 111:2490–98
231. Fernández-Alonso F, Bean BD, Zare RN. 1999. *J. Chem. Phys.* 111:1035–42
232. Fernández-Alonso F, Bean BD, Zare RN, Aoiz FJ, Bañares L, Castillo JF. 2001. *J. Chem. Phys.* 114:4534–45
233. Muga JG, Levine RD. 1989. *Chem. Phys. Lett.* 162:7–13
234. Allison TC, Friedman RS, Kaufman DJ, Truhlar DG. 2000. *Chem. Phys. Lett.* 327:439–45
235. Deleted in proof
236. Deleted in proof
237. Case DA, McClelland GM, Herschbach DR. 1978. *Mol. Phys.* 35:541–73
238. Hall GE, Houston PL. 1989. *Annu. Rev. Phys. Chem.* 40:375–405
239. Orr-Ewing AJ, Zare RN. 1994. *Annu. Rev. Phys. Chem.* 45:315–66
240. Orr-Ewing AJ, Zare RN. 1995. In *Advanced Series in Physical Chemistry*, ed. K Liu, A Wagner, pp. 936–1063. Singapore: World Sci.
241. Brouard M, Simons JP. 1995. In *Advanced Series in Physical Chemistry*, ed. K Liu, A Wagner, pp. 795–841. Singapore: World Sci.
242. Loesch HJ. 1995. *Annu. Rev. Phys. Chem.* 46:555–94
243. 1991. *J. Phys. Chem.* 95:7961–8422
244. 1997. *J. Phys. Chem. A* 101:7461–90
245. Aoiz FJ, Brouard M, Enriquez PA. 1996. *J. Chem. Phys.* 105:4964–82
246. Rakitzis TP, Kandel SA, Zare RN. 1997. *J. Chem. Phys.* 107:9382–91
247. de Miranda MP, Clary DC. 1997. *J. Chem. Phys.* 106:4509–21
248. de Miranda MP, Clary DC, Castillo JF, Manolopoulos DE. 1998. *J. Chem. Phys.* 108:3142–53
249. Kandel SA, Alexander AJ, Kim ZH, Zare RN, Aoiz FJ, et al. 2000. *J. Chem. Phys.* 112:670–85
250. Simpson WR, Rakitzis TP, Kandel SA, Lev-On T, Zare RN. 1996. *J. Phys. Chem.* 100:7938–47
251. Orr-Ewing AJ, Simpson WR, Rakitzis TP, Kandel SA, Zare RN. 1997. *J. Chem. Phys.* 106:5961–71
252. Kandel SA, Rakitzis TP, Lev-On T, Zare RN. 1996. *J. Chem. Phys.* 105:7550–59
253. Kandel SA, Rakitzis TP, Lev-On T, Zare RN. 1996. *Chem. Phys. Lett.* 265:121–28
254. Kandel SA, Rakitzis TP, Lev-On T, Zare RN. 1998. *J. Phys. Chem. A* 102:2270–73
255. Rakitzis TP, Kandel SA, Lev-On T, Zare RN. 1997. *J. Chem. Phys.* 107:9392–405
256. Fernández-Alonso F, Bean BD, Ayers JD, Pomerantz AE, Zare RN. 2000. *Z. Phys. Chem.* 214:1167–86
257. de Miranda MP, Aoiz FJ, Bañares L, Sáez Rábanos V. 1999. *J. Chem. Phys.* 111:5368–83

258. Lanziserra DV, Valentini JJ. 1995. *J. Chem. Phys.* 103:607–17
259. Metz RB, Bradforth SE, Neumark DM. 1992. *Adv. Chem. Phys.* 81:1–61
260. Krause JL, Kulander KC, Light JC, Orel AE. 1992. *J. Chem. Phys.* 96:4283–92
261. Bruckmeier R, Wunderlich C, Figger H. 1994. *Phys. Rev. Lett.* 72:2550–53
262. Azinovic D, Figger H. 1997. *Z. Phys. D* 42:105–12
263. Azinovic D, Bruckmeier R, Wunderlich C, Figger H, Theodorakopoulos G, Petsalakis ID. 1998. *Phys. Rev. A* 58:1115–28
264. Mahapatra S, Köppel H. 1998. *Phys. Rev. Lett.* 81:3116–19
265. Mahapatra S, Köppel H. 1998. *J. Chem. Phys.* 109:1721–33
266. Datz S. 2001. *J. Phys. Chem. A* 105:2369–73
267. Jensen MJ, Pedersen HB, Safvan CP, Seiersen K, Urbain X, Andersen LH. 2001. *Phys. Rev. A* 63:(5)2701–5
268. Strasser D, Lammich L, Krohn S, Lange M, Kreckel H, et al. 2001. *Phys. Rev. Lett.* 86:779–82
269. Kokoouline V, Greene CH, Esry BD. 2001. *Nature* 412:891–94
270. Müller U, Cosby PC. 1999. *Phys. Rev. A* 59:3632–42
271. Müller U, Eckert T, Braun M, Helm H. 1999. *Phys. Rev. Lett.* 83:2718–21
272. Mistrík I, Reichle R, Helm H, Müller U. 2000. *Phys. Rev. A* 63:042711–10
273. Cosby PC, Helm H. 1988. *Phys. Rev. Lett.* 61:298–301
274. Müller U, Cosby PC. 1996. *J. Chem. Phys.* 105:3532–50
275. Aberth W, Schnitzer R, Anbar M. 1975. *Phys. Rev. Lett.* 34:1600–3

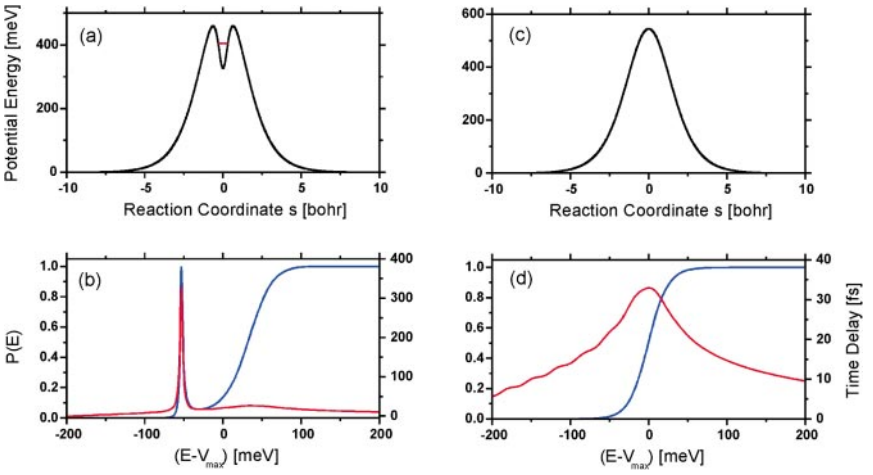

Figure 1 (*a*) Potential energy profile along the reaction coordinate displaying a well at the center. (*b*) Transmission probability P(E) (*blue curve*, left axis) and time delay (*red curve*, right axis) as a function of (E-V_{max}), where E is the total energy and V_{max} is the maximum value of the potential energy. The resonance peak below threshold at approximately -50 meV corresponds to the energy level of the well shown by the horizontal red line in (*a*). Panels (*c*) and (*d*) correspond to an Eckart barrier displaying no well along the potential energy profile. The potential parameters have been chosen so as to mimic as closely as possible the MEP for the $H + H_2$ reaction.

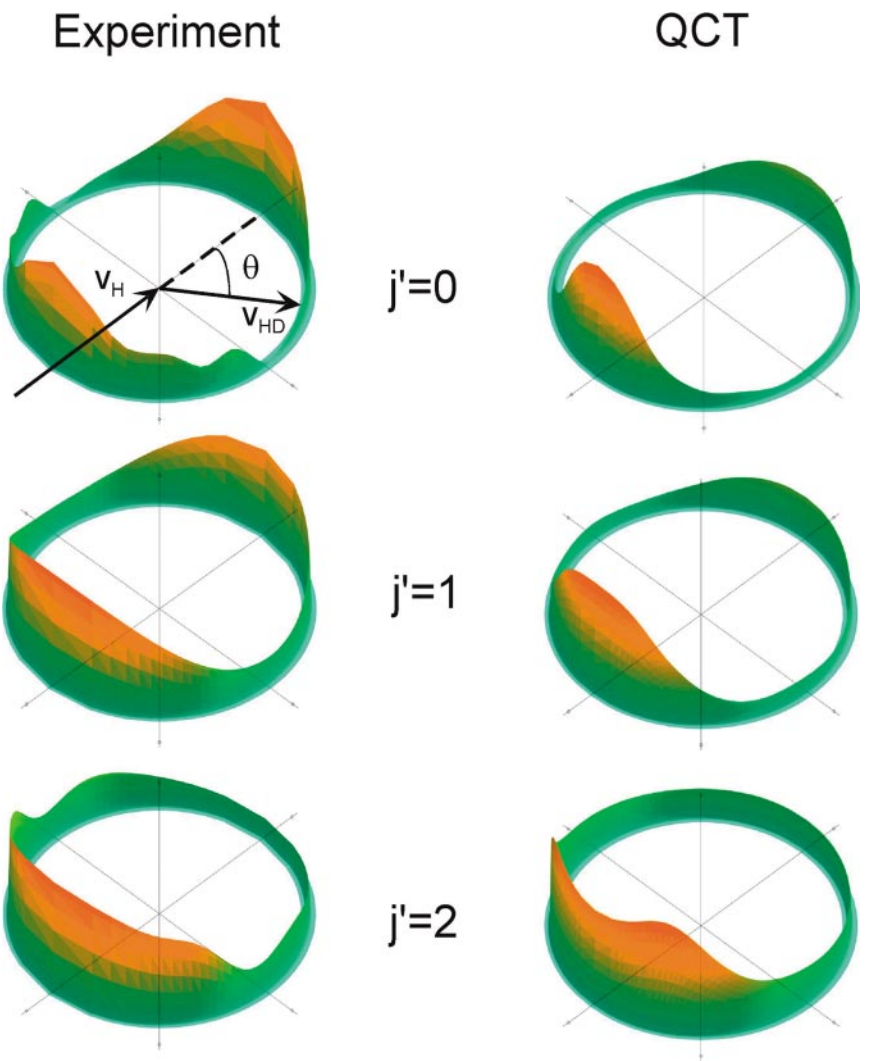

Figure 4 Polar plots of the HD($v' = 3$, $j' = 0$–2) center-of-mass differential cross sections from experiment (*left*) and QCT calculations (*right*) at $E_{col} = 1.64$ eV. The top polar plot on the left indicates with arrows the directions of reagents and products.

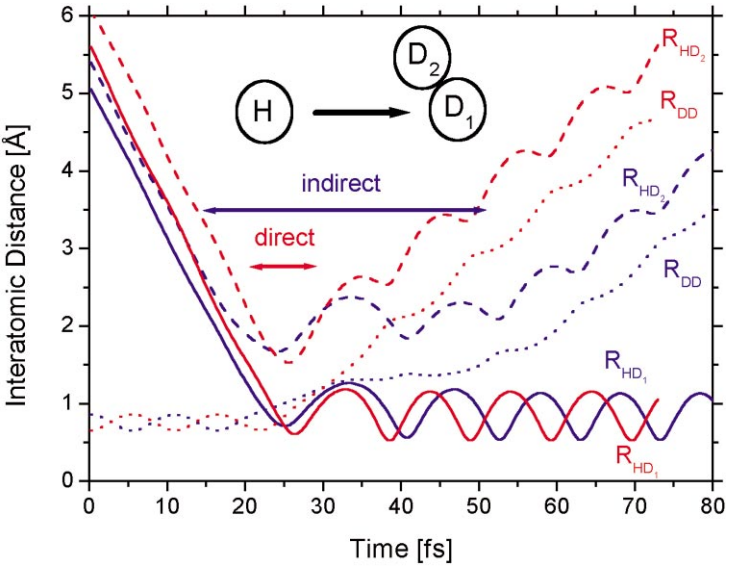

Figure 5 Temporal evolution of interatomic distances for $H + D_2(v = 0,\ j = 0) \rightarrow HD(v' = 3;\ j' = 0) + D$ at 1.64 eV obtained from QCT calculations. The *blue curves* represent an indirect trajectory that is forward scattered; the *red curves* represent a direct trajectory that is back scattered. The slope of the curves is the distance covered per unit time, that is, their relative velocity. Bars mark the approximate interaction time during which the complex hangs together.

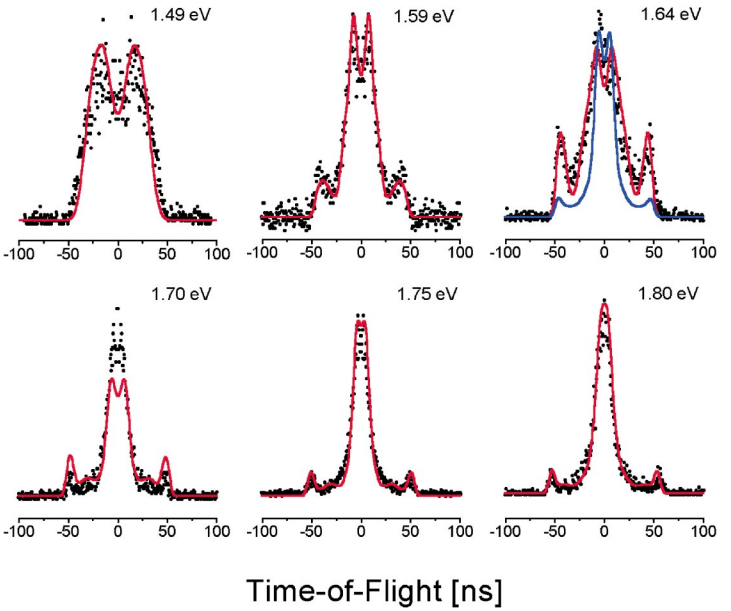

Figure 6 HD($v' = 3$, $j' = 0$) experimental time-of-flight profiles (*black circles*) as a function of collision energy. The *solid red lines* are the result of a forward convolution of the QM DCS calculations. At $E_{col} = 1.64$ eV, the *blue line* corresponds to the forward-convoluted time-of-flight profile for the QCT DCS.

Annual Review of Physical Chemistry
Volume 53, 2002

CONTENTS

Frontispiece—*Ignacio Tinoco, Jr.* xiv

PHYSICAL CHEMISTRY OF NUCLEIC ACIDS, *Ignacio Tinoco, Jr.* 1

HIGHER-ORDER OPTICAL CORRELATION SPECTROSCOPY IN LIQUIDS, *John T. Fourkas* 17

TIME-RESOLVED PHOTOELECTRON ANGULAR DISTRIBUTIONS: CONCEPTS, APPLICATIONS, AND DIRECTIONS, *Tamar Seideman* 41

SCATTERING RESONANCES IN THE SIMPLEST CHEMICAL REACTION, *Félix Fernández-Alonso and Richard N. Zare* 67

VACUUM ULTRAVIOLET SPECTROSCOPY AND CHEMISTRY BY PHOTOIONIZATION AND PHOTOELECTRON METHODS, *Cheuk-Yiu Ng* 101

THE MOLECULAR HAMILTONIAN, *Henning Meyer* 141

REVERSIBLE POLYMERIZATIONS AND AGGREGATIONS, *Sandra C. Greer* 173

SCANNING TUNNELING MICROSCOPY STUDIES OF THE ONE-DIMENSIONAL ELECTRONIC PROPERTIES OF SINGLE-WALLED CARBON NANOTUBES, *Min Ouyang, Jin-Lin Huang, and Charles M. Lieber* 201

ELECTRON TRANSFER AT MOLECULE-METAL INTERFACES: A TWO-PHOTON PHOTOEMISSION STUDY, *X.-Y. Zhu* 221

AB INITIO MOLECULAR DYNAMICS WITH DENSITY FUNCTIONAL THEORY, *John S. Tse* 249

TRANSITION PATH SAMPLING: THROWING ROPES OVER ROUGH MOUNTAIN PASSES, IN THE DARK, *Peter G. Bolhuis, David Chandler, Christoph Dellago, and Phillip L. Geissler* 291

ELECTRONIC STRUCTURE AND CATALYSIS ON METAL SURFACES, *Jeff Greeley, Jens K. Nørskov, and Manos Mavrikakis* 319

CHEMICAL SHIFTS IN AMINO ACIDS, PEPTIDES, AND PROTEINS: FROM QUANTUM CHEMISTRY TO DRUG DESIGN, *Eric Oldfield* 349

REACTIVE COLLISIONS OF HYPERTHERMAL ENERGY MOLECULAR IONS WITH SOLID SURFACES, *Dennis C. Jacobs* 379

MOLECULAR THEORY OF HYDROPHOBIC EFFECTS: "SHE IS TOO MEAN TO HAVE HER NAME REPEATED," *Lawrence R. Pratt* 409

STUDIES OF POLYMER SURFACES BY SUM FREQUENCY GENERATION VIBRATIONAL SPECTROSCOPY, *Zhan Chen, Y. R. Shen, and Gabor A. Somorjai* 437

QUANTUM MECHANICAL METHODS FOR ENZYME KINETICS, *Jiali Gao and Donald G. Truhlar* 467

SURFACE FEMTOCHEMISTRY: OBSERVATION AND QUANTUM CONTROL OF FRUSTRATED DESORPTION OF ALKALI ATOMS FROM NOBLE METALS, *Hrvoje Petek and Susumu Ogawa* 507

CONNECTING LOCAL STRUCTURE TO INTERFACE FORMATION: A MOLECULAR SCALE VAN DER WAALS THEORY OF NONUNIFORM LIQUIDS, *John D. Weeks* 533

INDEXES

Author Index 563
Subject Index 591
Cumulative Index of Contributing Authors, Volumes 49–53 623
Cumulative Index of Chapter Titles, Volumes 49–53 625

ERRATA

An online log of corrections to *Annual Review of Physical Chemistry* chapters may be found at http://physchem.annualreviews.org/errata.shtml